frontiers | Frontiers in Water

TYPE Original Research
PUBLISHED 02 May 2024
DOI 10.3389/frwa.2024.1356994

OPEN ACCESS

EDITED BY
Xiaohui Yan,
Dalian University of Technology, China

REVIEWED BY
Alain Isabwe,
University of Michigan, United States
Stephen McCord,
McCord Environmental, United States

*CORRESPONDENCE
Naivy Dennise Rodal-Morales
✉ nrodalmorales@ucmerced.edu

RECEIVED 17 December 2023
ACCEPTED 15 April 2024
PUBLISHED 02 May 2024

CITATION
Rodal-Morales ND, Beutel M, Fuhrmann B, Defeo S, Hansen AM, Harmon T, Brower S and Pasek J (2024) Hydrology and oxygen addition drive nutrients, metals, and methylmercury cycling in a hypereutrophic water supply reservoir.
Front. Water 6:1356994.
doi: 10.3389/frwa.2024.1356994

Hydrology and oxygen addition drive nutrients, metals, and methylmercury cycling in a hypereutrophic water supply reservoir

Naivy Dennise Rodal-Morales[1]*, Marc Beutel[1], Byran Fuhrmann[1,2], Shelby Defeo[1], Anne M. Hansen[3], Thomas Harmon[1], Sarah Brower[4] and Jeffery Pasek[4]

[1]Environmental Systems Graduate Group, University of California, Merced, CA, United States, [2]SePRO Corporation, EutroPHIX Division, Whitakers, NC, United States, [3]Mexican Institute of Water Technology, Morelos, Mexico, [4]City of San Diego Public Utilities Department, San Diego, CA, United States

Impaired water quality in Mediterranean climate reservoirs is mainly associated with eutrophication and internal nutrient loading. To improve water quality in hypereutrophic Hodges Reservoir, California, United States, a hypolimnetic oxygenation system (HOS), using pure oxygen gas, was implemented in 2020. This study encompasses 3 years of pre-oxygenation data (2017–2019) and 2 years of post-oxygenation data (2020–2021) to understand the cycling of nutrients, metals, and mercury in the reservoir. During the wet year of 2017, mildly reduced conditions lasted until mid-summer in the enlarged reservoir. Nutrients and metals were seen in the hypolimnion including ammonia (~2 mg-N/L), manganese (~0.5 mg/L), phosphate (~0.5 mg-P/L), and sulfide (~10 mg/L). Production of methylmercury (MeHg), an important bioaccumulative toxin, was favored from April to June with a hypolimnetic accumulation rate of around 200 ng/m^2·d. In contrast, the dry year of 2018 exhibited higher hypolimnetic concentrations of ammonia (~4 mg-N/L), manganese (~1 mg/L), phosphate (>0.5 mg-P/L), and sulfide (>15 mg/L). The rapid onset of highly reduced conditions in 2018 corresponded with low MeHg hypolimnetic accumulation (~50 ng/m^2·d). It seems that mildly reduced conditions were associated with higher MeHg accumulation, while sulfidic, reduced conditions impaired inorganic mercury bioavailability for MeHg production and/or promoted microbial demethylation. Sulfide also appeared to act as a sink for iron via FeS precipitation, and potentially for manganese via MnS precipitation or manganese coprecipitation with FeS. Mass flux estimates for 2017–2019 indicate that much of the nutrients that accumulated in the hypolimnion moved via turbulent diffusion into the epilimnion at loading rates far exceeding thresholds predicting eutrophic conditions. After oxygenation in 2020–2021, the reservoir water column was highly oxidized but showed a lack of thermal stratification, suggesting reservoir operations in combination with HOS implementation inadvertently mixed the water column in this relatively shallow reservoir. Post-oxygenation, concentrations of ammonia, phosphate, manganese, and mercury in bottom waters all decreased, likely in response to oxidized conditions. Oxygenated bottom waters exhibited elevated nitrate, a byproduct of ammonia nitrification, and iron, a byproduct of FeS oxidation, indicating a lake-wide response to oxygenation.

KEYWORDS

hypolimnetic oxygenation, iron cycle, methylmercury, internal nutrient loading, nitrogen cycle, hydrology

1 Introduction

Water quality management in water supply reservoirs is a significant topic for water security as climate factors and growing populations continue to exacerbate pressure on water availability (United States Environmental Protection Agency (USEPA), 2023). Eutrophication, and the subsequent algae decay that results in deoxygenation of deeper zones, is the main concern for productive lakes, especially during periods of stratification. Under these anaerobic conditions, associated with low oxidation–reduction (redox) potential, sediments tend to liberate ammonia, manganese, phosphate, iron, and in extreme cases, sulfides, degrading raw water quality (Beutel, 2006). In addition, internal nutrient loading, in which nutrients accumulate in bottom waters and diffuse or mix into the photic zone, can reinforce eutrophication. Simultaneously, the accumulation of iron may trigger harmful algal blooms (Leung et al., 2021; Molot et al., 2021), while manganese and iron can complicate drinking water treatment (Krueger et al., 2020). Anaerobic conditions also promote the activity of anaerobic bacteria such as sulfate- and iron-reducing bacteria (SRB, FeRB) that produce toxic methylmercury (MeHg) (Watras, 2009). This organic form of mercury (Hg) readily bioaccumulates in fish resulting in a health threat to wildlife and humans (Mergler et al., 2007).

Another important factor to consider when studying nutrients and metals cycling in reservoirs is the contribution of hydrology, particularly now that extreme hydrological events are increasing in frequency due to climate change. The consequences of these changes are variable and dependent on lake depth, surface area, mixing regime, and trophic status. In California, climate change predictions indicate a higher likelihood of droughts (Goss et al., 2020), but also an increase in the strength of atmospheric rivers and associated precipitation events (Mosley, 2015; Payne et al., 2020). Consequently, extreme droughts can increase the relative importance of internal nutrient loading as external loading diminishes, and lower water levels increase the mixing of nutrient-rich bottom waters into the photic zone (Mosley, 2015). Conversely, high precipitation and runoff from atmospheric rivers translate into elevated external nutrient and sediment loading. Hydrology is also closely related to Hg cycling in reservoirs because more frequent wetting and drying of littoral sediment correlates with MeHg levels in biota (Bigham et al., 2017; Seelos et al., 2021). Thus, to improve surface water treatability, while having the recreational and environmental benefits of a clean water reservoir, reservoir managers need to understand nutrients, metals, and Hg cycling, and the factors that play a role in their potential management.

The biogeochemical processes that occur during hypolimnetic deoxygenation mostly take place at the sediment–water interface (Figure 1). When algae die, sink, and are deposited onto profundal sediment, they are decomposed by bacteria consuming dissolved oxygen (DO). Ammonia is produced by the mineralization of organic matter (Forsberg, 1989) and accumulates when nitrification is inhibited under anoxic conditions (Rysgaard et al., 1994). Manganese is also released due to microbial dissolution of manganese-oxides (Davison, 1993; Munger, 2016). Phosphate and iron are released from the sediment to overlaying water by reductive dissolution of iron-oxides and release of associated phosphate (Golterman, 2001; Søndergaard et al., 2003). Finally, sulfide is produced by anaerobic microorganisms such as SRB. These anaerobic bacteria also produce toxic MeHg (Gilmour et al., 2013), which tends to build up in anoxic bottom waters of lakes and reservoirs (Regnell and Watras, 2019; Beutel et al., 2020; Poulin et al., 2023). In addition, inorganic Hg(II) and MeHg can accumulate in bottom waters when metal oxides are dissolved and release sorbed Hg (Chadwick et al., 2006; Beutel et al., 2020).

One strategy to limit the accumulation of reduced compounds in bottom waters and suppress internal nutrient loading in reservoirs is the addition of pure oxygen gas to bottom waters using hypolimnetic oxygenation systems (HOS) (Beutel and Horne, 1999; Bierlein et al., 2017; Austin et al., 2019). These engineered systems are capable of adding large amounts of DO to the bottom of reservoirs (1–100 metric tons/d), while maintaining thermal stratification, with a relatively small infrastructure size, energy, and cost (Beutel and Horne, 1999). In 2020, the City of San Diego (CSD) installed a HOS in Hodges Reservoir, California, United States, to enhance the quality and treatability of reservoir water. With few management options to lower MeHg levels in fish, water managers are also interested in the potential for HOS to suppress the buildup of MeHg in bottom waters and lower subsequent bioaccumulation into the aquatic food web (Beutel et al., 2020; Eckley et al., 2020).

The study aimed to assess patterns of nutrients, metals, and Hg cycling, over the study period of the years 2017–2021, combining water quality monitoring by the University of California Merced (UCM) and CSD. Key objectives and working hypothesis of this multi-year study included: (1) to assess impacts of interannual variations in hydrology (e.g., wet versus dry years) on nutrients, metals, and Hg cycling. During dry years, we hypothesized to see shallower and warmer waters that favor rapid deoxygenation of bottom waters and enhanced accumulation rates of nutrients and metals in the hypolimnion; (2) to evaluate, the impacts of HOS operation on conventional water quality parameters including nitrogen, phosphorus, iron, and manganese, and on the cycling of Hg in the water column. As these compounds are redox-sensitive, their accumulation in the hypolimnion was expected to decrease with the oxidized conditions after HOS implementation; and (3) to determine accumulation rates of nutrients and metals in bottom waters and their subsequent transfer via turbulent diffusion from the hypolimnion to the epilimnion (i.e., internal nutrient loading). The objective was to quantify the changes in internal nutrient loading after oxygenation. We hypothesized that the internal loading would decrease post-oxygenation, which would translate into water quality improvement.

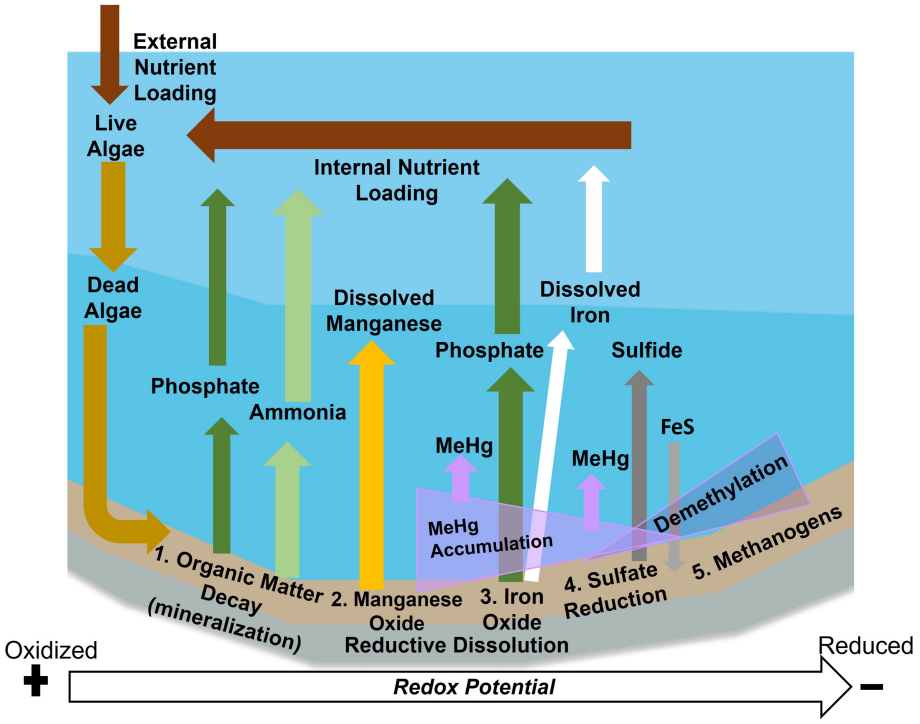

FIGURE 1
Anoxic biogeochemical processes at the sediment–water interface in reservoirs. External nutrient loading leads to sediment accumulation and decay of organic matter, which can release ammonia (light green) and phosphate (dark green) via mineralization. As sediments become mildly reduced metal oxides undergo reductive dissolution, resulting in manganese (yellow), iron (white) and phosphate (dark green) release. These processes lead to internal nutrient loading. Under reduced conditions sulfide is released (dark gray) and can precipitate with iron (light gray). Toxic methylmercury (MeHg) (purple) tends to be released under mildly reduced conditions but lost under highly reduced conditions.

2 Methods

2.1 Study site

Hodges Reservoir, located in Northern San Diego County, California, United States is a water supply reservoir for the Santa Fe Irrigation District (SFID) and the San Dieguito Water District, which serve around 15,000 people in the region of Rancho Santa Fe and Solana Beach. The reservoir also serves as a backup water source for CSD and San Diego County Authority. In addition, Hodges Reservoir is part of a pumped storage system in which water is pumped up to nearby Olivenhain Reservoir and released back to Hodges Reservoir to supply power during peak electrical demands. Hydropower production is predicated on maintaining a reservoir surface elevation of around 89 m above mean sea level (amsl). At this elevation, the reservoir has a maximum depth of 19.2 m, a mean depth of 6.4 m, and a surface area of 2.3 km^2.

Summertime water temperatures are typically around 25°C in surface waters and 16°C in bottom waters. The region has a precipitation season from October to March and hot, dry summers typical of a Mediterranean climate. Precipitation in the watershed feeds inflows that increase the surface water elevation by 2–6 m annually in wet years. The trophic state of Hodges Reservoir is categorized as hypereutrophic with sulfate-rich waters. The reservoir's main inflow is the San Dieguito River which yields relatively high external nutrient loading from a large watershed (641 km^2). But during dry summer and fall periods, eutrophication is likely driven by internal nutrient loading. Based on past water quality monitoring, Hodges Reservoir exhibits poor water quality, including low water transparency (Secchi depth < 1 m) and elevated total chlorophyll (chl) levels in surface waters (> 60 µg/L) (Beutel et al., 2020). Warmer temperatures in the reservoir, predicted by climate change models, will result in longer and stronger thermal stratification, which will exacerbate internal nutrient loading and eutrophication (Lee and Biggs, 2015). For Hg, the predominant source is atmospheric deposition resulting in low total Hg (THg) levels in sediments typical of California background levels (< 0.05 µg/g dry weight). Nonetheless, Hodges Reservoir is listed on the Clean Water Act Section 303(d) List for elevated levels of Hg in fish (Beutel et al., 2020).

As is typical for hypereutrophic reservoirs, Hodges Reservoir has an anoxic hypolimnion during the warmer months (May–October) and is well mixed during winter (November–April) after the fall turnover. Under typical operating conditions (water surface elevation of 89 m amsl), the reservoir has a relatively low Osgood index (ratio of mean depth in m to square root of surface area in km^2) of around 4, suggesting it is not strongly thermally stratified during summer and fall (Cooke et al., 2013). In fact, the reservoir is known to exhibit polymictic characteristics during periods with maximum depths less than 15 m (Lee and Biggs, 2015). We also estimated the lake number (L_N), a dimensionless parameter indicative of mixing potential in lakes and reservoirs based on Robertson and Imberger (1994) using rLakeAnalyser function in RStudio. Under typical stratified summer conditions, the L_N was around 14 with average wind speed (~2.2 m/s) and around 3 with high wind speed (~4.5 m/s). During fall, L_N was

around 0.9 with average wind speed (~6.2 m/s). L_N values indicate moderate stratification strength in summer and low stratification strength in the fall when the lake overturns each year. Hence nutrients presumably diffuse and/or mix into surface waters during summer stratification and fall turnover, supporting algal productivity.

To lower internal nutrient loading and improve raw water quality and treatability, in March of 2020 the CSD installed a "Speece Cone" HOS with a delivery capacity of 6 metric tons/d (Figure 2A; Horne and Beutel, 2019). This delivery rate was determined based on a detailed assessment of sediment oxygen demand and water column oxygen demand in the reservoir prior to HOS installation (Beutel, 2015). The HOS includes a 49.3 m^3 (13,000 gal) on-shore liquid oxygen storage tank and an evaporator unit to convert the liquid to gas, and a 6 m-tall, submerged cone with a 100-horsepower intake pump secured to the bottom of the reservoir at a depth of around 14.5 m. Oxygen gas is released at the top of the cone which acts as a counter-current contact chamber, resulting in around 95% oxygen transfer efficiency. A 30-m-long pipe diffuser connected to the bottom of the cone discharges oxygenated water with elevated DO (~70 mg/L) horizontally above the sediments into the hypolimnion all year long. The HOS was not installed in the deepest part of the reservoir due to infrastructure constraints including limited access to power.

2.2 Field monitoring

Field monitoring was carried out from 2017 to 2021 as a collaborative effort between UCM and CSD. The study analyzes 4 years (2017–2019, 2021) of monthly water column data collected by UCM and 5 years (2017–2021) of approximately weekly to monthly

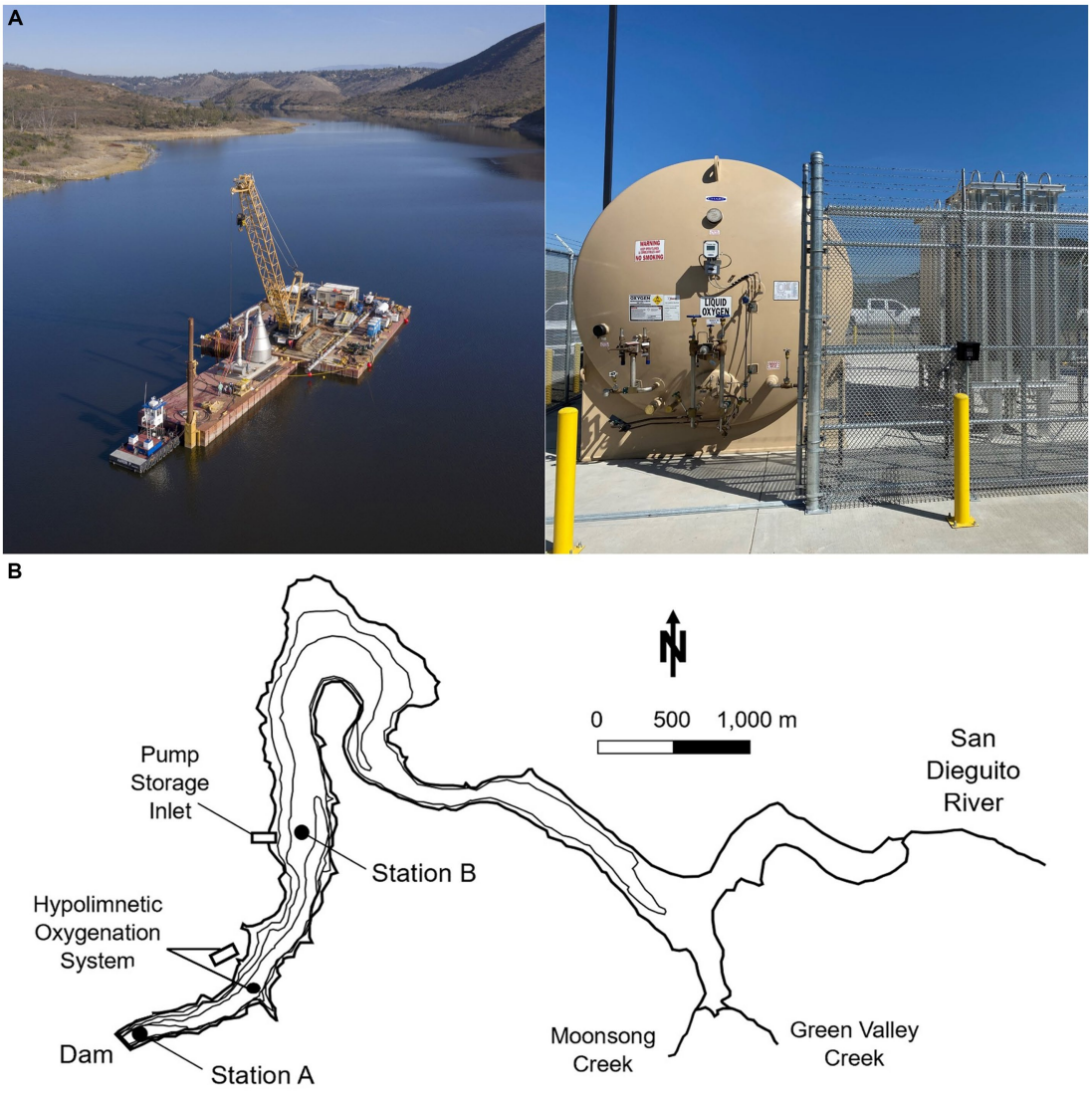

FIGURE 2
(A) Picture of the oxygenation cone on construction barge before being submerged (left), and on-shore facilities including liquid oxygen storage tank and evaporators (right). Photo credit: City of San Diego. **(B)** Map of Hodges Reservoir, showing the two sampling stations A and B, location of the pumped storage system, and location of the hypolimnetic oxygenation system. Contours are every 5 m and mapped water surface elevation is of ~91 m. Modified from Beutel et al., 2020.

water quality data collected by CSD (Table 1). Water samples were collected at two monitoring stations (Figure 2B). Station A was located at the deepest zone of the reservoir (~19 m depth) near the dam, and station B (~12 m depth) was located about 2 km upstream close to the pump storage connection.

UCM samples were obtained with a 1.2-l Polytetrafluoropolymer Kemmerer sampler every 3 m in depth from the surface to the bottom of the reservoir, including an additional near-bottom water sample (~0.5 m from the bottom), from March/April to October/November. UCM monitored for ammonia, nitrate, phosphate measured as soluble reactive phosphorus (SRP), total phosphorus (TP), iron, manganese, sulfate, chloride, sulfide, dissolved organic carbon (DOC), MeHg, and THg. Hg sampling used the dirty-clean-hands method 1669 with Hg clean Teflon water sampler and 250 mL certified clean bottles (USEPA, 1996). Sulfide samples were preserved in the field with zinc acetate and sodium hydroxide. In the laboratory, nutrients (ammonia, nitrate, and phosphate), anions (sulfate and chloride), and DOC samples were preserved by filtering through prewashed 0.45 µm filters and kept inside a freezer. Water samples for unfiltered iron and manganese were preserved with nitric acid (1.0%) and refrigerated. THg and MeHg samples were preserved with hydrochloric acid (0.4%) and refrigerated. Field data also included Secchi depth and chl measurements in samples collected at 0, 3, 6, and 9 m depth. Chl samples were filtered onto GFC filters and placed inside the freezer for later extraction and analysis.

The CSD monitoring included weekly sampling for DO, pH, redox potential, and temperature at station B from 2017 to 2021, and occasional monitoring at station A during the summer months, using a YSI-EX02 multiparameter water quality sonde (YSI Corporation, Yellow Springs, OH, United States). Geosmin, a taste and odor compound produced by phytoplankton that complicates water treatment, was measured weekly at station B, and sporadically at station A, from 2017–2021. Hydrological data (e.g., rainfall, surface elevation, runoff, discharge) used to manage water elevation in Hodges Reservoir were collected monthly by CSD. Rainfall data were calculated based on an evaporation pan measurement that was scaled to the surface area of the reservoir. CSD also monitored monthly water quality in the surface, mid-depth coinciding with a key water outlet at an elevation of 83.8 m amsl (compared to typical water surface elevation of ~89 m amsl), and bottom waters for ammonia, nitrate, phosphate, iron, and manganese at station B, and sporadically at station A, from 2017–2021.

2.3 Analytical methods

Water quality analyses on UCM samples were performed at the UCM Environmental Analytical Laboratory using standard methods (APHA, 2023). Dissolved nutrients (ammonia, nitrate, phosphate, TP) were analyzed on a LACHAT QuikChem 8500 autoanalyzer using standard colorimetric methods by air-segmented continuous-flow absorption spectrophotometry. TP samples were digested via acid persulfate digestion before colorimetric analysis for SRP. Reporting limits were 0.02 mg-N/L for ammonia, 0.05 mg-N/L for nitrate, and 0.02 mg-P/L for SRP and TP. Iron and manganese were determined by inductively coupled plasma optical emission spectrometry on an Optima 5300 DV ICP-OES with a reporting limit of 0.01 mg/L. Sulfate was measured using ion chromatography on an Agilent 7500cs mass spectrometer with a reporting limit of 0.5 mg/L. Sulfide was analyzed by iodometric titration with a reporting limit of 0.4 mg/L. Chl as total

TABLE 1 Average bottom water quality at station A and B for pre-oxygenation years 2017–2019 and post-oxygenation years 2020–2021.

		2017		2018		2019		2020		2021	
Parameter		A	B	A	B	A	B	A	B	A	B
Ammonia, mg-N/L	CSD		2.5 ± 1.2		3.2 ± 2.5		3.0 ± 1.6	0.22	0.25 ± 0.17	0.2	0.13 ± 0.07
	UCM	1.9 ± 1.2	1.9 ± 0.9	4.3 ± 3.1	2.8 ± 1.2	2.4 ± 1.6	2.1 ± 1.2			0.05 ± 0.2	0.01 ± 0.14
Nitrate, mg-N/L	CSD		0.1 ± 0.2		0.1 ± 0.1		0.3 ± 0.3	0.22	0.51 ± 0.76	0.16	0.13 ± 0.1
	UCM	0.1 ± 0.06	0.03	ND	ND	0.05 ± 0.02	0.03 ± 0.01			0.32 ± 0.2	0.23 ± 0.1
Phosphate, mg-P/L	CSD		0.8 ± 0.5		0.5 ± 0.2		0.1 ± 0.04	0.22	0.39 ± 0.07	0.9	0.7 ± 0.12
	UCM	0.5 ± 0.1	0.5 ± 0.05	1.0 ± 0.33	0.7 ± 0.1	0.5 ± 0.14	0.8 ± 0.1			0.10 ± 0.04	0.13 ± 0.07
Iron, mg/L	CSD		0.1 ± 0.02		0.1 ± 0.03		0.1 ± 0.02	0.19	0.21 ± 0.12	0.1	0.4 ± 0.3
	UCM	0.1 ± 0.02	0.1 ± 0.02	0.05 ± 0.03	0.04 ± 0.03	0.03 ± 0.01	0.3 ± 0.01			0.17 ± 0.09	0.17 ± 0.12
Manganese, mg/L	CSD		0.5 ± 0.1		0.8 ± 0.2		1.1 ± 0.3	0.18	0.16 ± 0.05	0.31	0.23 ± 0.09
	UCM	0.5 ± 0.1	0.5 ± 0.08	0.9 ± 0.1	0.6 ± 0.2	0.8 ± 0.3	0.7 ± 0.2			0.27 ± 0.4	0.13 ± 0.1
Total Hg, ng/L	UCM	3.4 ± 0.9	3.8 ± 0.4	1.4 ± 0.2	1.1 ± 0.2	2.1 ± 1.4	1.7 ± 0.3			0.58 ± 0.3	0.53 ± 0.3
Methyl-Hg, ng/L	UCM	1.4 ± 0.4	1.5 ± 0.5	0.2 ± 0.07	0.3 ± 0.09	0.4 ± 0.3	0.5 ± 0.2			0.04 ± 0.01	0.05 ± 0.01
Sulfate, mg/L	UCM	162 ± 13.2	159 ± 7.1	60 ± 10.5	65 ± 8.22	168 ± 17.7	175 ± 16.1			104 ± 24.3	140 ± 86.6
Sulfide, mg/L	UCM	3.7 ± 3.9	2.9 ± 2.4	14.6 ± 8.7	10.3 ± 5.3	11.5 ± 0.3	5.4 ± 4.5			ND	ND
DOC, mg/L	UCM	10.4 ± 0.9		9.3 ± 0.36	9.7 ± 0.8					8.62 ± 0.23	

The values represent the average plus/minus standard deviation from May to September of the bottom waters. Data from City of San Diego (CSD) and UC Merced (UCM). For UCM data, bottom waters are considered the deepest three depths sampled ($n \sim 15$). For CSD data, bottom waters were collected weekly at station B ($n \sim 20$). For CSD data in 2020 and 2021, bottom waters were collected 1 week in July at station A. ND is not detected. DOC is dissolved organic carbon.

chlorophyll was analyzed using the standard 90% acetone extraction method. DOC was measured using the combustion catalytic oxidation method on a Shimadzu TOC-V analyzer. THg analysis was performed on a MERX-T (Brooks Rand Labs, Seattle, WA, United States) using cold vapor atomic fluorescence spectroscopy (CVAFS) based on method 1631 (USEPA, 2002). Samples for MeHg analysis were distilled (2 h at 125°C with nitrogen gas flow <50 mL/min) before being measured on a MERX-M (Brooks Rand Labs, Seattle, WA, USA) using ethylation, gas chromatography, and CVAFS based on the method 1630 (USEPA, 2001). Hg analyses followed strict quality control standards including method blanks (<0.1 ng/L), matrix spikes (75–125% range), analytical duplicates, and ongoing procedure recovery (75–125% range). Reporting limits were 0.2 ng/L for THg and 0.02 ng/L for MeHg.

Water quality analyses on CSD samples were performed at the San Diego Water Quality Laboratory following standard methods (APHA, 2023). Phosphate was measured via ion chromatography with a reporting limit of 0.02 mg-P/L. Total ammonia was measured using the phenate colorimetric with a reporting limit of 0.03 mg-N/L. Nitrate was measured with the NED dihydrochloride colorimetric method with a reporting limit of 0.05 mg-N/l. Unfiltered iron and manganese were measured on an Agilent 7900 ICP-MS with a reporting limit of 0.01 mg/L for iron and 0.2 mg/L for manganese. Geosmin was measured via SM6040D using solid-phase microextraction and gas chromatography/mass spectrometry with a reporting limit of 5 ng/L.

2.4 Data analysis

To assess patterns of nutrients and metals accumulation in the hypolimnion of Hodges Reservoir, at each sampling station we calculated the rate of areal mass accumulation between sampling events, termed the monthly hypolimnetic accumulation rate (MHAR) (mg/m²·d) using Equation 1:

$$\mathrm{MHAR} = \frac{\Delta C_H * h_H}{\Delta t} \quad (1)$$

where ΔC_H (g/m³) is the increase or decrease in hypolimnetic mean concentration between monthly sampling events, h_H (m) is the height of the hypolimnion, and Δt (d) is the time between monthly sampling events. The height of the hypolimnion was estimated from the thermocline to the bottom of the reservoir at the sampling station. The height of the hypolimnion was typically 13–14 m at station A and 8–9 m at station B.

The second part of the data analysis encompassed the application of a 1-D model using a mass transport equation based on the heat-accumulation method described by Chapra (1997). The lake is modeled as a mixed surface layer (epilimnion) overlaying a bottom layer (hypolimnion) separated by a thin transitional layer (metalimnion). Compounds released from anoxic sediment (e.g., ammonia, phosphate, MeHg) accumulate in the hypolimnion and then move across the metalimnion via turbulent diffusion. The flux J (g/m²·d), termed here in the context of lake management as "internal nutrient loading," is estimated using Equation 2:

$$J = -E_t \frac{dC}{dx} \quad (2)$$

where dC/dx (mg/L/L) is the concentration gradient across the metalimnion estimated as the concentration in the upper hypolimnion minus the concentration in the epilimnion, dx (m) is the metalimnion thickness (typically around 2 m), and E_t (cm²/d) is the vertical diffusion coefficient. We estimated site-specific diffusion coefficients for Hodges Reservoir by first estimating the heat exchange coefficient (v_t, cm/d) based on the observed rate of warming of the hypolimnion using Equation 3:

$$v_t = \frac{V_h}{A_t * t_s} \ln\left(\frac{T_e - T_{hi}}{T_e - T_{hs}}\right) \quad (3)$$

where V_h (m³) is the volume of the hypolimnion, A_t (m²) is the area of the thermocline, T_e (°C) is the average epilimnion temperature, T_{hi} (°C) is the hypolimnion temperature at the beginning of summer (typically May–June), T_{hs} (°C) is the hypolimnion temperature during strong summer stratification (typically May to September), and t_s (d) is the number of days during the strong stratification. The internal nutrient loading for a given month can then be estimated using Equation 2 because the vertical diffusion coefficient (E_t) is equivalent to the heat exchange coefficient (v_t) multiplied by the thickness of the metalimnion (dx).

3 Results

3.1 Hydrology

The water balance in Hodges Reservoir is composed of inflows including runoff, direct precipitation, and imported water, and outflows including evaporation and withdrawal for potable water delivery and elevation management. Consequently, runoff driven by regional precipitation strongly affects the water budget. An assessment of annual precipitation near Hodges Reservoir shows an overall mean of around 350 mm (1940–1962 and 2010–2020, Western Regional Climate Center, 2023; World Weather Online, 2023). Years experiencing abundant rainfall register precipitation levels above 500 mm, while drier years are associated with values below 100 mm per year. Precipitation was 584 mm in 2017, 130 mm in 2018, 430 mm in 2019, and 160 mm in 2021. Accordingly, in the context of this study, we categorized each of these years as wet, dry, average, and dry, respectively. Based on hydrologic data from CSD, the water balance in water year 2019 (October–September), an average precipitation year, includes runoff of 11.9 million m³/y, evaporative losses of 3.3 million m³/y, and withdrawal for potable water delivery and elevation management of 8.6 million m³/y. Mean reservoir volume in 2019 water year was 18,102,026 m³ and water residence time was around 1.5 y. In wet 2017 water year, runoff increased to 25.1 million m³/y, and water residence time decreased to around 0.9 y. In dry 2018 water year, runoff was around 1.1 million m³/y, and water residence time increased to around 16.4 y. Regional rainfall and associated runoff also affect the size of the hypolimnion, which was shown in this study to be an important controller of nutrients and metals cycling in Hodges Reservoir. The hypolimnion volume at the end of spring was around 10,087,000 m³ in wet 2017, but only 4,293,000 m³ in dry 2018.

During this multi-year study, precipitation and water surface elevation showed a wide range of variation. In 2016, rainfall was

minimal at around 200 mm, and water surface elevation was steady at around 89 m amsl (Figure 3). Winter of 2016 and spring of 2017 showed elevated precipitation of more than 450 mm. High precipitation corresponded with significant runoff into the reservoir and an increase in elevation to 94 m amsl reflected by April. Then, the elevation decreased throughout the year, as no external runoff occurred, and water was transferred from the reservoir via withdrawals and raw water deliveries. The low precipitation and runoff in 2018 combined with continued water releases resulted in a steady drop in elevation from around 90 m amsl at the start of the year to around 89 m amsl by the end of the year. 2019 had high precipitation during February–March (250 mm) and runoff increased the elevation to 93 m amsl. Water elevation decreased to 89 m amsl by the end of the year via withdrawals and raw water deliveries. 2020 and 2021 had low precipitation and the elevation showed a quasi-steady state of around 89 m amsl.

3.2 Field parameters

From 2017 to 2019, surface water temperature at stations A and B was around 14°C at the beginning of the year and warmed up to 25–30°C during the summer months (Figures 4, 5). The thermocline formed between 5 and 7 m depth (14–16 m above the bottom) at station A and between 3 and 5 m (7–9 m above the bottom) at station B (Figure 4). After stratification, formed during summer, bottom water temperature warmed up from 14°C to 18°C (Figures 4, 5). In 2020–2021 after HOS implementation, at both stations A and B, there was only a very slight thermocline formation, and the entire water column was around 24–25°C during summertime (Figures 4, 5). From 2017–2019, pH at stations A and B decreased with depth during the summer months with surface water values between 8 and 9.5 and bottom water values between 7 and 8 (Figure 4). pH values were lower in magnitude and exhibited a less dramatic vertical gradient down the water column in 2020–2021. 2018 had the highest summertime pH in surface water (9.3) while 2021 had the lowest (8.1).

From 2017 to 2019, DO in surface water was 5–9 mg/L during summer months at station A. The DO decreased dramatically below the thermocline, going anoxic at 4–6 m deep in 2017 and 2018, and at 8 m deep in 2019 (Figure 4). After HOS implementation in 2020, DO showed a steady decrease down the water column from around 7 mg/L in surface waters to 0 mg/L near the bottom at a depth of 18 m. In 2021, DO showed no dramatic vertical variation with values of 6 mg/L on the surface and 4–5 mg/L in the bottom water. At station B, DO profiles for 2017–2019 looked similar with surface water values of around 9 mg/L and anoxia below 5 m deep (Figures 4, 5). After HOS operation in 2020–2021, DO increased to around 2 mg/L between a depth of 5–8 m. Then, DO decreased to 0 mg/L below 8 m deep (Figures 4, 5). Redox potential at both stations A and B during 2017–2019 was indicative of oxidized conditions (>200 mV) in surface waters and reduced conditions (−300 to −350 mV) in bottom waters (Figures 4, 5). After the HOS operation in 2020–2021, conditions throughout the water column at stations A and B were oxidized (>300 mV) (Figures 4, 5). Redox potential showed a decrease in deep water samples near the sediment–water interface, especially in 2021 at station B (−10 mV at 12 m) (Figure 4). The yearly patterns at station B showed low redox conditions coincident with anoxia in bottom waters from 2017 to 2019, and elevated redox potential throughout the water column in 2021 (Figure 5). Finally, Secchi disk transparency typically ranged from 60 and 100 cm in all study years (Table 2).

3.3 Water chemistry

3.3.1 Nutrients, chlorophyll, and dissolved organic carbon

From 2017–2019 at stations A and B, ammonia concentration progressively increased in bottom waters during the summer months

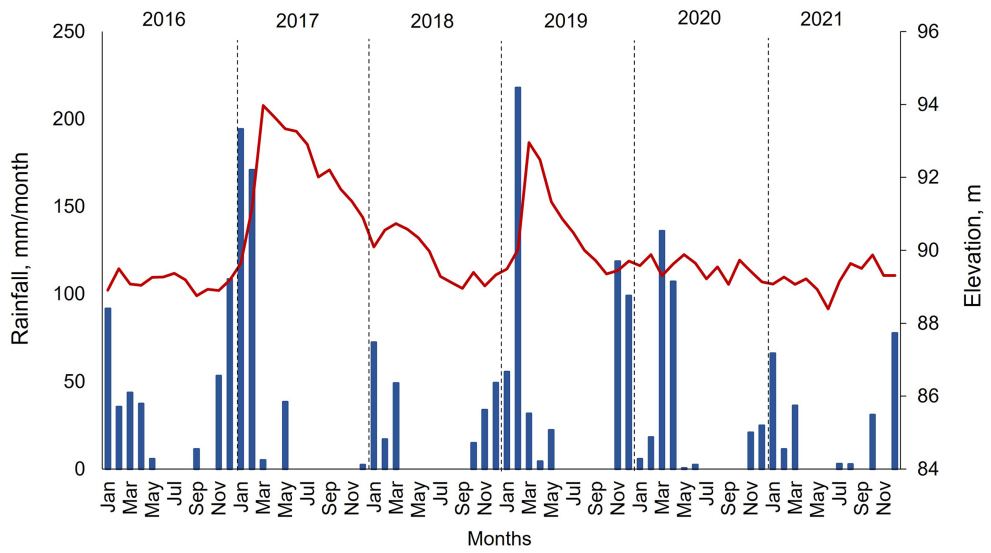

FIGURE 3
Monthly rainfall (blue bars) and surface elevation (red line) in Hodges Reservoir from 2016 to 2021. Data collected monthly by the City of San Diego. Rainfall represents calculated values based on an evaporation pan measurement that is scaled to the surface area of the reservoir.

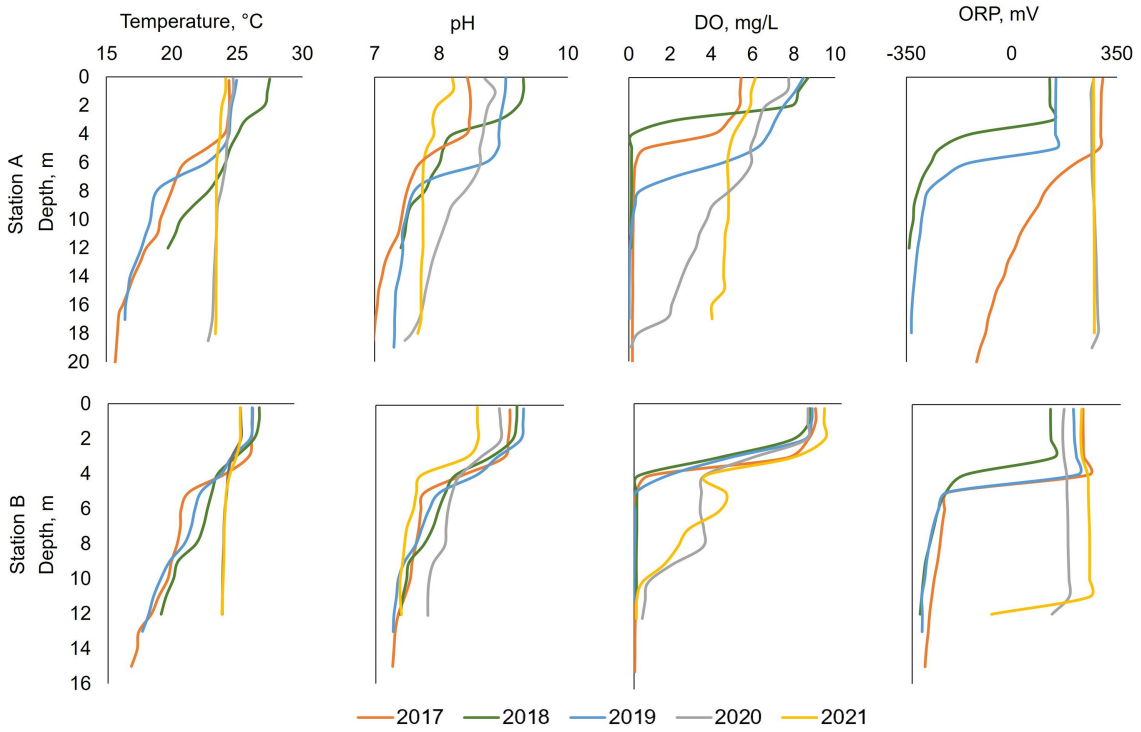

FIGURE 4
Summer (July or August) profiles at stations A and B from left to right: temperature, pH, dissolved oxygen (DO), and redox potential (ORP). Oxygenation occurred during 2020 and 2021. Note that in 2018 at station A data was only collected to a depth of 12 m.

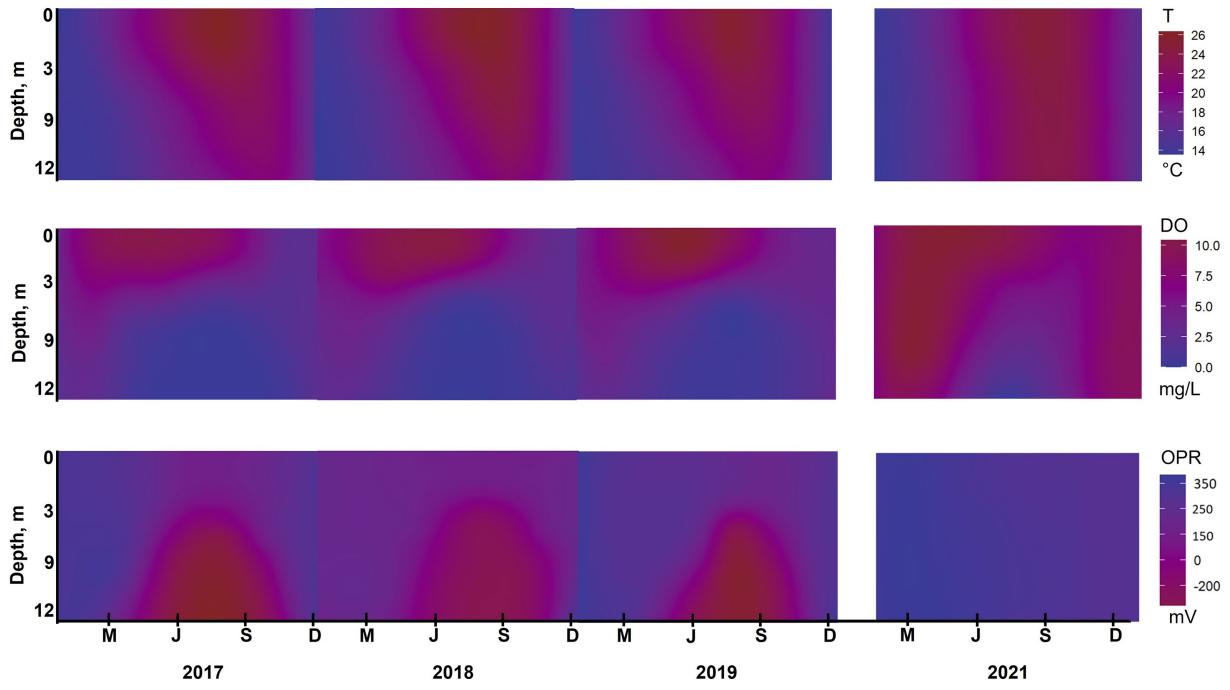

FIGURE 5
Water quality isopleths for temperature (T), dissolved oxygen (DO) and redox potential (ORP) at station B during 2017–2019 and 2021. The isopleths were calculated as an annual interpolation of weekly data collected by the City of San Diego from January through December to a depth of 12 m using RStudio. Note actual elevation of reservoir varied between years; see text for details.

TABLE 2 Surface water quality during summer months, May to September, for pre-oxygenation years 2017–2019 and post-oxygenation year 2021.

	2017		2018		2019		2021	
Parameter	A	B	A	B	A	B	A	B
Total Chl, µg/L	61 ± 19 (n = 5)	74 ± 16 (n = 5)	66 ± 40 (n = 4)	73 ± 32 (n = 4)	92 ± 52 (n = 5)	145 ± 101 (n = 5)	29 ± 11 (n = 5)	37 ± 3 (n = 5)
Total Chl mass, g/m^2	0.52		0.58		1.03		0.24	
Total P, mg/L	0.14 ± 0.03 (n = 5)	0.15 ± 0.02 (n = 5)	0.29 ± 0.08 (n = 4)	0.26 ± 0.02 (n = 4)	0.21 ± 0.03 (n = 5)	0.19 ± 0.04 (n = 5)	0.11 ± 0.02 (n = 5)	0.11 ± 0.01 (n = 5)
Sechi Disk, cm	74 ± 18 (n = 5)		67 ± 20 (n = 4)	62 ± 16 (n = 4)	110 ± 99 (n = 5)	100 ± 102 (n = 5)	70 ± 22 (n = 5)	
Geosmin, ng/L		ND (n = 9)		35 (n = 18)		18 (n = 31)		ND (n = 28)

Values are means, except for geosmin values which are medians, and sample size is noted in parentheses. For chlorophyll and total phosphorus, surface waters represent the average from 0 to 9 m deep at station A, and from 0 to 6 m deep at station B. For chlorophyll mass, before oxygenation was considered 0–9 m, after oxygenation (2021) was considered all the water column. ND is not detected.

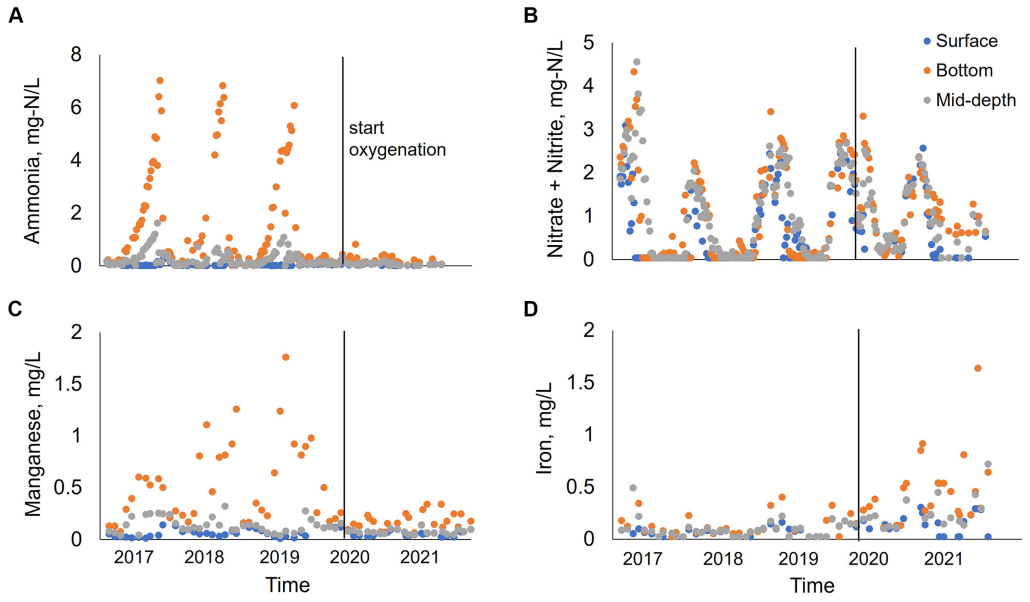

FIGURE 6
Water quality parameters of ammonia **(A)**, manganese **(B)**, nitrate + nitrite **(C)**, and iron **(D)** at station B for 2017–2021. Data collected by the City of San Diego from January to December at three different depths: surface, bottom and mid-depth.

peaking at 7–7.5 mg-N/L, followed by a decrease in concentration starting in October (0.05 mg-N/L) (Figures 6, 7). At station B, surface and metalimnion ammonia concentrations were low throughout the year (Figure 6A). Nitrate concentrations showed the opposite behavior, with levels peaking at the beginning of spring (0.4 mg-N/L at station A; 3.5–4.5 mg-N/L at station B) and decreasing with the onset of stratification, being depleted during the summer months throughout the water column (Figures 6B, 7). In 2020, when oxygenation started, ammonia and nitrate patterns shifted. There was no ammonia in bottom waters during summer months, while nitrate concentration was low but not depleted (~0.5 mg-N/L) (Figure 7). In 2021, ammonia concentration was almost depleted (~0.3 mg-N/L) throughout the water column, while nitrate progressively increased in the water column during the winter–spring months (Figures 6A,B, 7). Peak nitrate concentrations were around 1 mg-N/L at station A and 3 mg-N/L at station B. From July to September 2021, nitrate concentration at stations A and B was low in the surface and metalimnion samples but slightly elevated (~0.5 mg-N/L) in bottom water (Figures 6B, 7).

Phosphorus cycling was consistent for 2017–2019 at station A (Figure 7). Phosphate progressively increased in the hypolimnion through the stratified period, with higher concentrations at the end of summertime (September–October). During these 3 years, phosphate concentrations were around 0.5 mg-P/L starting at 5 m deep to the bottom from May to August. 2018 showed the highest phosphate concentration of around 2 mg-P/L in the hypolimnion, followed by 2019 with 1.3 mg-P/L, and 2017 with 0.8 mg-P/L (Figure 7). TP showed the highest concentration (~0.4 mg-P/L) in surface waters (0–5 m) in 2018, compared to 2017 (0.1 mg-P/L) and 2019 (0.2 mg-P/L), indicating high algae productivity all year (Table 2; Figure 7). Still, it seems that whole-lake total chl mass, estimated based on reservoir bathymetry and chl profiles down the water column from

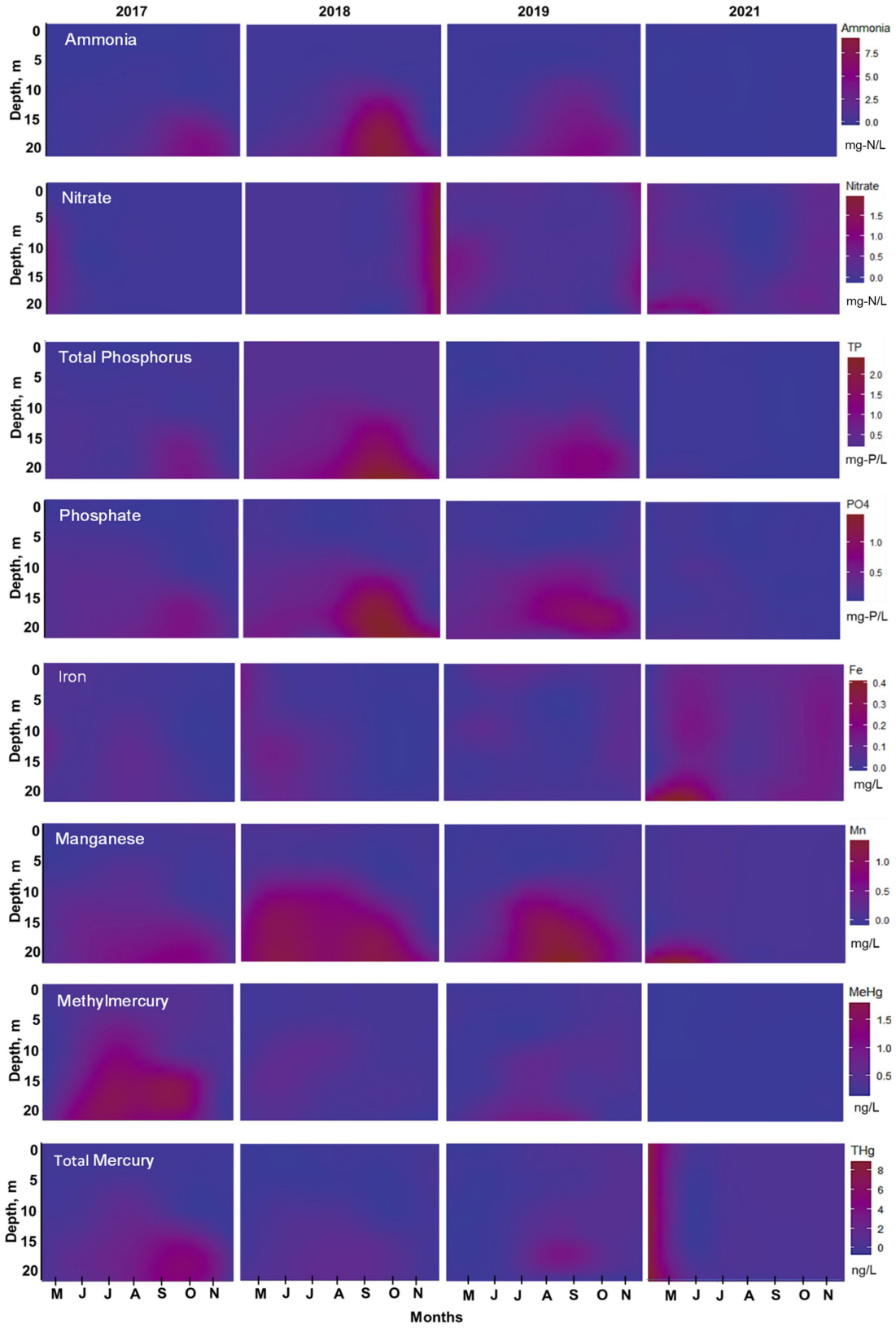

FIGURE 7
Water quality isopleths from top to bottom at station A: ammonia, nitrate, total phosphorus, phosphate, iron, manganese, methylmercury, and total mercury for 2017–2019, and 2021. Data collected monthly by UC Merced at 3-m-deep intervals April through November and interpolated to a depth of 20 m using RStudio. Note actual elevation of reservoir varied between years; see text for details.

June to August, showed higher mass in 2019 (1.03 g/m^2) compared to 2018 (0.58 g/m^2) and 2017 (0.52 g/m^2). However, 2018 chl mass was only calculated considering June and July months due to missing data so it might be underestimated (Table 2). In the hypolimnion, TP followed the same pattern as phosphate indicating that most of the phosphorus present in bottom waters is in the soluble reactive form (Figure 7). On the contrary, after oxygenation in 2021, TP and phosphate concentrations were low (<0.2 mg-P/L) during the entire sampling season throughout the water column (Figure 7; Table 2). DOC concentrations in bottom waters did not change dramatically after oxygenation. During 2017 and 2018, DOC values were around 9.8 mg/L, whereas in 2021, DOC was slightly lower with a concentration of 8.6 mg/L (Table 1). Chl levels in surface waters were typically 60–150 µg/L in 2017–2019 and 30–40 µg/L in 2021 (Table 2). The taste and odor compound geosmin appeared to be elevated in 2017–2019 relative to 2021 after HOS operation (Table 2).

3.3.2 Metals

From 2017 to 2019, manganese concentration progressively increased in bottom waters with the onset of hypolimnetic anoxia, peaking between 0.8–1.8 mg/L before fall turnover in November when concentrations decreased to around 0.2 mg/L throughout the water column (Figures 6C, 7). Patterns at station B from 2017 to 2019 also showed a vertical increase in concentration down the water column (Figure 6C). However, the years showed different patterns of peak concentrations in the hypolimnion (Figures 6C, 7). In 2017, the peak concentration in the hypolimnion (~0.6 mg/L) was in July and August. 2018 peak manganese concentration in the bottom waters (~1.2 mg/L) was observed in May–July and again in September–October. In 2019, peak manganese concentration (1.3–1.8 mg/L) was observed in August–September. After oxygenation, manganese concentrations were lower in bottom waters (~0.3 mg/L). However, at station A in 2021, there was a peak manganese concentration of 1 mg/L during May–June (Figure 7). This was not seen at station B where the highest concentration in the bottom waters during 2021 was 0.3 mg/L (Figure 6C).

Iron behavior was opposite to manganese during the summertime before and after oxygenation. From 2017–2019, iron concentration was low throughout the water column (0.02 mg/L station A; 0.2 mg/L station B). Iron concentration increased in the hypolimnion during May, July, and August and decreased by the end of the summer months (Figures 6D, 7). 2019 also showed an interesting pattern with the highest iron concentration in surface waters at station A in the spring (Figure 7). After oxygenation, 2020–2021, iron concentration was elevated throughout the water column at both stations, an order of magnitude higher than under pre-oxygenation years (0.4 mg/L station A, and 2 mg/L station B) (Figures 6D, 7). In 2021 after oxygenation, iron had two peaks of elevated concentration in the water column (Figure 7). The first peak was in the hypolimnion in May–June at station A (0.4 mg/L) and in April at station B (0.8 mg/L). The second peak was at the end of the summer months in the water column at station A (0.25 mg/L) and in August in the hypolimnion at station B (0.7–1.8 mg/L) (Figures 6D, 7).

3.3.3 Mercury

For 2017–2019, patterns of Hg concentration in the hypolimnion at station A were different according to the year (Figure 7). The wet year of 2017 had the highest MeHg concentration (>1.5 ng/L) present in bottom waters from May to October. THg peak concentration (~6.5 ng/L) happened from September to November (Figure 7). On the contrary, the dry year of 2018 had the lowest Hg concentration. MeHg (<1 ng/L) was observed in bottom waters only during May and June and THg (~2 ng/L) was observed from June to October. In 2019, MeHg (~ 3 ng/L) was observed from June to October and THg (~5 ng/L) from August to September (Figure 7). After oxygenation in 2021, MeHg was below the reporting limit in the bottom waters, while THg concentration throughout the water column was around 1 ng/L (Figure 7).

3.4 Internal loading dynamics

We calculated MHAR for ammonia, phosphate, manganese, THg, and MeHg at stations A and B for the study period (Figure 8). The highest accumulation rates for nutrients and metals were generally seen during the dry year 2018, while the highest THg and MeHg accumulation rate was seen during the wet year 2017. Focusing on the pre-oxygenation years of 2017–2019, ammonia MHAR showed similar patterns in all years with rates increasing as summer progressed. Ammonia MHAR typically ranged from 50 to 300 mg/m^2·d, but 2018 showed a massive accumulation in July on the order of 1,000 mg/m^2·d at station A. For phosphate, there was a continued accumulation throughout the summer months with values ranging from 10 to 80 mg/m^2·d and generally peaking in June/July. Manganese seemed to have a progressive accumulation of 30–250 mg/m^2·d, which generally stopped in June/July, except for 2018 when it stopped in May. THg accumulation started in May, with values ranging from 100 to 400 ng/m^2·d, and typically exhibited a loss (negative MHAR) during August. 2018 had the lowest THg accumulation with values <100 ng/m^2·d. MeHg MHAR patterns for 2017–2019 showed a progressive accumulation that ended in June with values ranging from 50 to 350 mg/m^2·d, followed by a loss during July/August, and a small accumulation in September. 2018 also had the lowest MeHg accumulation rate with only around 50 ng/m^2·d during May. In general, the values calculated from the MHAR were the same order of magnitude as anoxic fluxes measured in chamber experiments with Hodges Reservoir water and sediment conducted previously by Beutel et al. (2020).

Results of the internal loading calculation at station A, which estimated the rate of transport of nutrients and metals across the thermocline for 2017–2019, showed similar heat exchange coefficients (V_t) (1.2–1.6 cm/d) and vertical diffusion coefficient (E_t) values (0.003 cm^2/s) for all years (Table 3). Typical vertical diffusion coefficient values for moderately deep systems with mean depths of 5–10 m range from 0.003–0.009 cm^2/s (Chapra, 1997). The wet year of 2017 appeared to have the lowest average fluxes of internal loading of phosphate, ammonia, and manganese, while the dry year of 2018 had the lowest internal loading of MeHg. 2019 had average precipitation during the year but had higher internal nutrient loading values compared to the wet year of 2017, except for MeHg. 2017 and 2019 exhibited a loss of nitrate while 2018 showed nitrate depletion since June. We present the contrasting patterns of internal loading dynamics for June for the wet year, 2017, and the dry year, 2018 (Figure 9). Values of MHAR and mass transport to the epilimnion were generally on the same order of magnitude, even though the two values were calculated using very different approaches. In general,

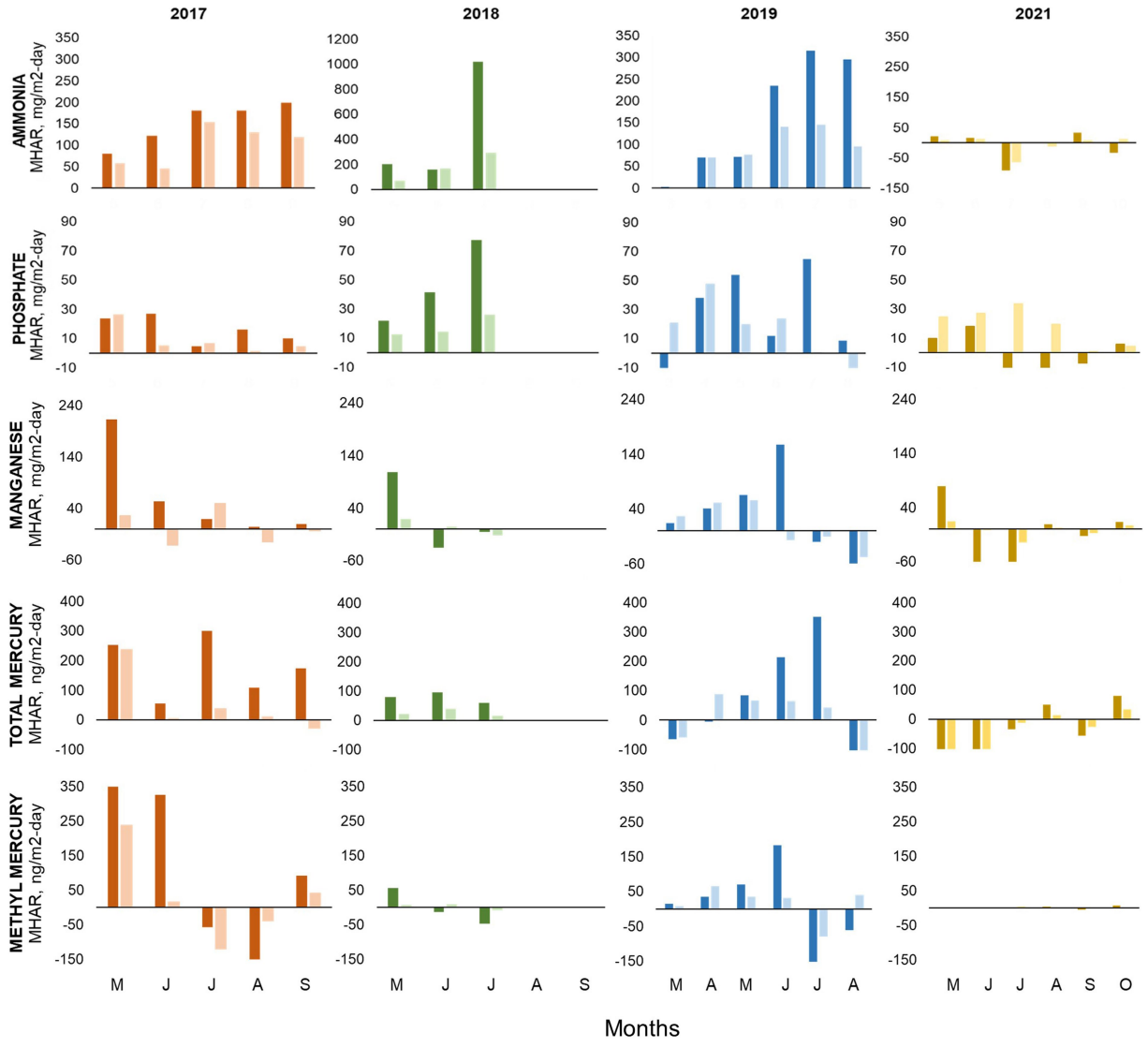

FIGURE 8
Monthly Hypolimnetic Accumulation Rate (MHAR), top to bottom: ammonia, phosphate, manganese, total mercury, and methylmercury at station A (bright color) and B (light color) during 2017, 2018, 2019 and 2021. Data used for the calculation were collected monthly by UC Merced at 3-m-deep intervals from April through November.

there was double the magnitude of MHAR and internal nutrient loading for ammonia and phosphate in 2018 compared to 2017, whereas values for MeHg and manganese were higher in 2017 compared to 2018. In addition, MeHg showed a higher transport through the thermocline in 2017, which was associated with higher bioaccumulation into seston and zooplankton (Beutel unpublished). Negative values of MHAR and internal nutrient loading for manganese and MeHg in 2018 suggest a manganese and MeHg sink in bottom waters.

After oxygenation in 2021, we barely observed any accumulation of ammonia, phosphate, manganese, THg, and MeHg based on our MHAR assessment (Figure 8). Any accumulation that happened at the beginning of the season was followed by loss and a small release in October. Phosphate showed an interesting pattern of continuous accumulation (30 $mg/m^2 \cdot d$) at station B. But as the water column appeared more mixed in 2021, this calls into question the appropriateness of applying the MHAR metric, since it assumed accumulation into a well-defined hypolimnion. Therefore, we used a whole-lake mass approach (McCord et al., 2016) to assess two parameters of interest, TP and MeHg, which are relatively conservative on a whole-lake basis. We estimated the whole-lake mass of TP and unfiltered MeHg in Hodges Reservoir based on bathymetry and concentration down the water column. We comparing July 2019, the average precipitation year, with July 2021, after oxygenation with relatively mixed conditions. 2019 hypolimnetic TP mass of around 4,867 kg (19,026,000 m^3 lake volume; 1.8 mg/L volume-weighted mean concentration) was higher than the 2021 whole-lake TP mass of around 2,084 kg (14,262,000 m^3; 0.55 mg/L). For MeHg, in 2019, hypolimnetic mass of around 2 g (19,026,000 m^3; 1.18 $\mu g/m^3$) volume-weighted mean concentration was higher than the 2021 whole-lake MeHg mass of around 0.6 g (14,262,000 m^3; 0.22 $\mu g/m^3$).

4 Discussion

4.1 Nitrogen cycle

At the sediment–water interface of hypereutrophic reservoirs, the nitrogen cycle is dominated by mineralization, the formation of ammonium from the degradation of organic matter, and denitrification, the microbial transformation of nitrate into nitrogen gas. We can observe these two processes being dominant in Hodges Reservoir in 2017–2019. Ammonia progressively accumulated in the hypolimnion while nitrate was depleted early in the season as anoxic conditions and redox potential favored these reactions. However, there are some differences in the nitrogen cycle among the years before oxygenation. 2017 and 2019 showed high nitrate concentrations in bottom waters (1–4.5 mg-N/L) at the beginning of the season and a progressive ammonia accumulation in the hypolimnion (MHAR ~200 mg/m^2·d). While 2018 showed low nitrate concentration (0.2–2 mg-N/L) in bottom waters at the beginning of the season, and higher ammonia MHAR (>250 mg/m^2·d) peaking in July (Figures 6–8).

Differences in nitrogen cycling year to year can be explained by the wet versus dry conditions (Figure 3). During the dry year 2018, there was negligible runoff resulting in low external nutrient loading and a relatively small lake volume. Upon the formation of the thermocline and the relatively small hypolimnion, DO was rapidly depleted and redox potential quickly dropped (Figures 4, 5). Thus, organic matter degradation promoted high ammonia MHAR (>200 mg/m^2·d) and high internal nutrient loading all year long (Figures 8, 9; Table 3). Nitrate was only seen at the end of the season due to the fall turnover event mixing ammonia from bottom water into an oxic water column where the nitrification process could occur (Figures 6B, 7). Interestingly, high nitrate concentration was seen at the beginning of the season of 2019 (Figures 6B, 7). On the contrary, the rain seen at the beginning of the years 2017 and 2019 brought runoff from the watershed that increased the volume of the reservoir and resulted in substantial external nutrient loading (Figure 3). The resulting hypolimnion was around two times the volume of the hypolimnion in dry year 2018, which meant that the hypolimnion started with a much higher mass of oxygen. In addition, lake waters had elevated levels of nitrate, a potent oxidant, due to the nitrification of large ammonia releases during the previous years, as well as elevated

TABLE 3 Internal nutrient loading average values for pre-oxygenation years 2017–2019.

Parameter	2017	2018	2019
Heat exchange coeff. (V_t), cm/d	1.23	1.39	1.59
Vertical Diffusion Coefficient (Et), cm^2/s	0.0028	0.0030	0.0030
Phosphate, mg-P/m^2·d	11	40	61
Ammonia, mg-N/m^2·d	53	150	168
Manganese, mg/m^2·d	10	38	71
Nitrate mg-N/m^2·d	−56	0	−27
Methylmercury, ng/m^2·d	39	7	16

Values calculated using a mass transport equation based on the heat-accumulation method described by Chapra (1997); see methods for more details. Values are average of monthly rates estimated for May to August ($n = 4$) for 2017 and 2019, and for May to July ($n = 3$) for 2018 due to missing sampling date.

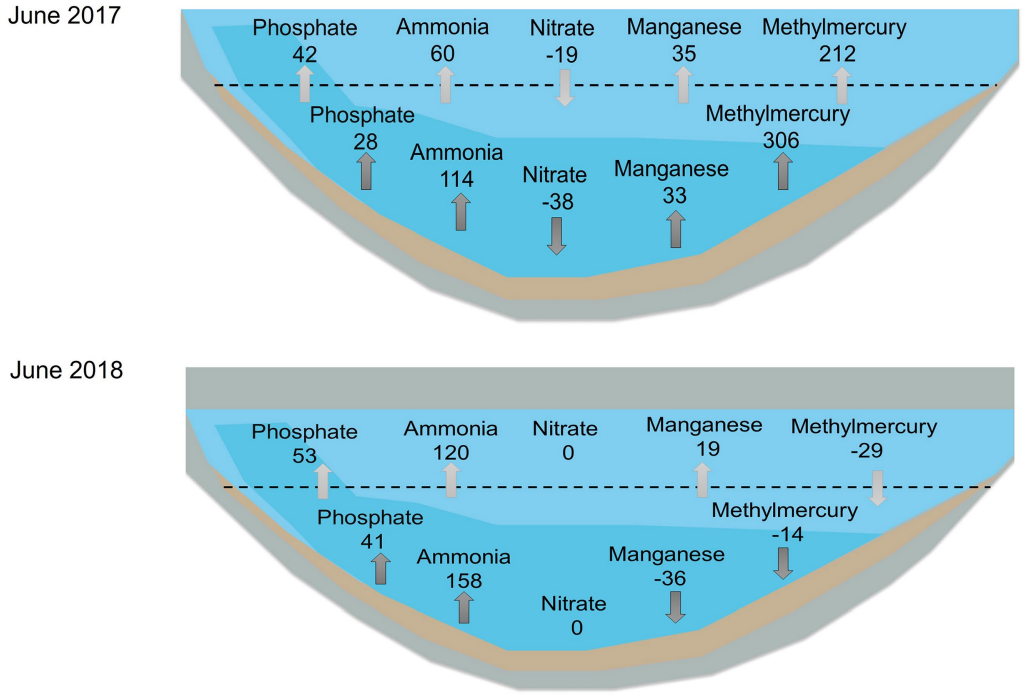

FIGURE 9
Example estimates of hypolimnetic accumulation (dark gray) and mass transfer across the thermocline (i.e., internal nutrient loading) (light gray) for the month of June for 2017 (top) and 2018 (bottom). Units are mg/m^2·d except for methylmercury which is ng/m^2·d. Note reservoir was substantially smaller in volume in 2018. From left to right: phosphate, ammonia, nitrate, manganese, and methylmercury. Dashed line represents the thermocline. Data used for the calculations were collected monthly monthly by UC Merced at 3-m-deep intervals from April through November.

levels of nitrate in stormwater inflows (1–2 mg-N/L) (City of San Diego, 2023). As a result, bottom water stayed aerobic with elevated redox levels for a longer time after stratification, resulting in less internal nutrient loading (Figures 5, 9; Table 3). By poising redox potential above that at which phosphate-containing iron-oxides in sediment undergo reductive dissolution, nitrate has been shown to be a potent inhibitor of sediment phosphorus release in a range of aquatic ecosystems (Beutel et al., 2016).

As expected, the nitrogen cycle pattern shifted after oxygenation starting in 2020. DO concentrations in bottom waters were around 2 mg/L and redox potential was >300 mV (Figures 4, 5). As a result, nitrification, the oxidation of ammonium to nitrate, was the dominant reaction (Rysgaard et al., 1994). Ammonia concentrations stayed low (0.3–0.5 mg-N/L) all year long throughout the water column (Figures 6A, 7). Nitrate concentrations, between 1 and 2 mg-N/L, were seen early in the season in bottom waters and stayed at low concentration (0.7 mg-N/L) throughout the water column the rest of the season. As there was weaker stratification, nitrate appeared to be mixed throughout the water column. However, there was lower nitrate concentration in the water column during July to September, which could be associated with higher water temperatures enhancing the activity of denitrifying organisms in anoxic sediments, and more algae growth in the surface waters (Figures 6B, 7). These results highlight the paradox of nitrogen cycling in eutrophic lakes: the addition of oxygen can indirectly stimulate the anaerobic process of denitrification (nitrate reduction to nitrogen gas) by promoting nitrification (ammonia oxidation to nitrate), resulting in the net loss of ammonia from the system. This phenomenon of net nitrogen loss has also been observed in Camanche Reservoir, California, United States, which has been oxygenated with a Speece Cone HOS since the early 1990s (Beutel, 2006; Horne and Beutel, 2019).

The difference in relative concentrations of ammonia and nitrate after oxygenation might have repercussions in the phytoplankton taxa seen in Hodges Reservoir. Ammonia is normally the preferred compound for algae and bacteria because of the smaller energy cost for assimilation, but eukaryotic phytoplankton are also able to use nitrate, giving them an advantage under nitrate-rich conditions (Harris et al., 2016). In contrast, high ammonia relative to nitrate favors cyanobacteria growth, especially non-nitrogen-fixing taxa, as well as the production of secondary metabolites such as the common taste and odor compound geosmin (Harris et al., 2016). These dynamics appear to be occurring in Hodges Reservoir. In 2021, when nitrate concentrations increased and ammonia concentration decreased, because of oxygen addition, geosmin measured at station B decreased compared to pre-oxygenation years (Figure 6B; Table 2). Another interesting observation is the apparent drop in nitrate concentrations in the water column at stations A and B in the summer of 2021, which appeared to correspond with an increase in chl under elevated iron concentration (Figures 6B,D, 7; Table 2). The loss of summertime nitrate may be linked to the presence of iron since iron is known to facilitate nitrate uptake and stimulate algal productivity in some phytoplankton communities (Havens et al., 2012; Robertson et al., 2016; Ma et al., 2021).

4.2 Manganese and iron cycling

Similar to nitrate and ammonia, manganese and iron had different behaviors between dry and wet years, as well as before and after oxygenation. Both manganese-oxides and iron-oxides in surficial sediment undergo reductive dissolution under reduced conditions, releasing reduced manganese (Mn(II)) and iron (Fe(II)) into overlaying water, with manganese-oxides being more susceptible to reductive dissolution as redox potential drops (Davison, 1993). For pre-oxygenation years, 2017–2019, manganese hypolimnetic accumulation was observed in all years, but patterns were different for each year and corresponded to the redox status of the system and the hydrology (Figures 4, 8). In the wet year 2017, in which hypolimnetic redox potential dropped slowly, modest manganese accumulation was observed from May to July resulting in low concentration in bottom water. This year also showed a late-season manganese flux in September, which could be associated with the abiotic reduction of refractory Mn-oxides by sulfide (Böttcher and Thamdrup, 2001; Beutel et al., 2020), as sulfide (>15 mg/L) was elevated during this period (Figure 8). In contrast, in dry year 2018, when redox potential dropped to low levels earlier in the year, manganese accumulation was observed only in May (Figure 8). This contrast is highlighted in Figure 9 where in June 2017 there was manganese accumulation in bottom waters (MHAR of 33 $mg/m^2 \cdot d$), whereas in June 2018 there was manganese loss (MHAR of -36 $mg/m^2 \cdot d$). A negative MHAR (manganese loss from the hypolimnion) was also observed later in the stratified season in 2019 (Figure 8). Two mechanisms could account for this observation. As discussed below, iron monosulfide minerals (mackinawite, FeS) likely precipitated under Fe(II)- and sulfide-rich conditions and may have scavenged Mn(II) from bottom waters (Morse and Luther III, 1999). Another possible sink for manganese could be precipitation with sulfide forming alabandite (MnS). This mineral is typically not observed in freshwaters due to its relatively high solubility product ($pK_{sp} \sim 0.4$) (Delfino and Lee, 1968; Davison, 1993). Solubility calculations ($pK_{sp} \sim 2.9$) suggest that MnS precipitation may have been favored at the end of summer in bottom waters of Hodges Reservoir under highly sulfidic (~30 mg/L) and manganese-rich (~1 mg/L) conditions.

Patterns of iron concentration in the hypolimnion before oxygenation (2017–2019) were less obvious than for manganese (Figures 6C,D, 7). A similar pattern of modest and sustained increase in concentration during wet 2017, compared to a more intense high concentration during dry 2018, was observed. But in all years, iron concentration diminished in the summer. It seems that the high sulfide concentrations, a byproduct of SRB activity in the relatively high sulfate waters (~200 mg/L) of Hodges Reservoir, favored FeS precipitation in the hypolimnion (Balistrieri et al., 1992; Luther et al., 2003; Wolthers et al., 2005). Typical concentrations of total sulfide (~15 mg/L) and total iron (~0.07 mg/L) in hypolimnetic water at station A under highly reduced conditions (-200 mV) were indicative of FeS precipitation based on the reported solubility product for FeS ($pK_{sp} \sim 3$) (Beutel, 2000). FeS precipitation was also observed during the anoxic phase of laboratory chamber experiments assessing sediment release of nutrients and metals in Hodges Reservoir under oxic versus anoxic conditions (Beutel et al., 2020).

Unlike manganese, iron cycling is linked to the internal loading of phosphorus since the dissolution of iron-oxides in sediment is commonly accompanied by the release of phosphate to overlaying water (Golterman, 2001; Søndergaard et al., 2003; Lovley et al., 2004). This linkage is difficult to see in the water quality dataset, since summertime hypolimnetic iron concentration is low (via FeS precipitation sink) when phosphate concentration is elevated,

especially in 2018 and 2019 (Figure 7). But this linkage between iron and phosphate release is more obvious in bottom waters during 2017, when the hypolimnion went anoxic more slowly and phosphate and iron concentrations in bottom waters increased from around July through August (Figure 7). In all years, elevated phosphate concentration was observed late in the season, presumably after more labile iron-oxides were reduced. This may be the result of abiotic reduction of refractory iron-oxides by sulfide under the highly sulfidic conditions of bottom waters in the late summer (Mitchell and Balwin, 1998; Zak et al., 2006). It also could be the result of the mineralization of decaying algae stimulated by the high rates of internal loading in this hypereutrophic reservoir (Forsberg, 1989). To put the magnitude of internal loading in context, we estimated annual rates of internal phosphate loading for Hodges Reservoir (~18–55 g-P/m^2-y). Values were two orders of magnitude higher than that predicting a eutrophic trophic status (~0.2 g-P/m^2-y) for this relatively shallow reservoir (mean depth ~ 6 m) using the Vollenweider phosphorus loading curve (Horne and Goldman, 1993).

Manganese and iron cycling appeared to change substantially after oxygenation. At both stations A and B for 2020–2021, manganese values in bottom water no longer showed an increase in concentrations as the season progressed. Instead, it showed low and steady concentrations suggesting some continued release via reductive dissolution of manganese-oxides, especially early in 2021 at station A (Figures 6C, 7). In contrast, iron concentration was elevated throughout the water column, but phosphate and TP were low (Figures 6D, 7). Since iron-oxide reductive dissolution typically results in the co-release of iron and phosphate (Golterman, 2001; Søndergaard et al., 2003), there appears to be another source of iron in bottom waters. The source of this iron could be the oxidation of FeS in surficial sediment. FeS is metastable and elevated DO and redox potential at the sediment–water interface can promote FeS dissolution, releasing dissolved Fe(II) which would result in Fe(III)-oxides formation (Chen and Morris, 1972; Wang et al., 2023). Freshly formed iron-oxides produced by Fe(II) oxidation in natural waters tend to exist primarily as colloids (1–100 nm), which are resistant to gravitational settling unless they aggregate and become large enough to sink (Chikanda et al., 2021). Moreover, iron-oxide colloids can bind with natural organic matter in waters with elevated carbon-to-iron molar ratios (>1.6) via bonding to the humic acids (Liao et al., 2017). DOC measured after oxygenation in Hodges Reservoir was around 8.5 mg/L, yielding a carbon-to-iron ratio of around 20, suggesting inhibition of humic acid/iron-oxide aggregation (Table 1). This is a possible explanation for the persistent concentrations of iron observed in the post-oxygenated water column (Figures 6D, 7). The mechanism of FeS oxidation forming iron-oxides to the water column, combined with the colloid nature of resulting iron-oxides in high DOC waters, could also explain elevated iron throughout the water column in the early spring during the years before oxygenation, especially in 2018 (Figure 7).

4.3 Methylation window

MeHg accumulation in aquatic environments is the result of the competition of two main cycling processes, Hg methylation and MeHg demethylation (Figure 1; Barkay and Gu, 2022). Hg methylation is performed mainly by anaerobic microorganisms and thus tends to occur under anaerobic conditions (Ullrich et al., 2001). But inorganic Hg(II) bioavailability for methylation tends to decrease as reducing conditions become more severe (Benoit et al., 1999; Regnell and Watras, 2019). As a result, Hg methylation to MeHg occurs at the redox boundary in aquatic sediment, which can coincide with SRB activity at the sediment–water interface (Gilmour et al., 2018). MeHg demethylation is prevalent under oxidized conditions and performed by aerobic microorganisms using the mer-detoxification pattern (Du et al., 2019). It is also performed by some SRB and methanogenic microorganisms under highly reduced conditions (Marvin-DiPasquale et al., 2000). As a result of these complex processes, peak MeHg production in aquatic ecosystems tends to occur under moderately anaerobic and mildly reduced conditions (e.g., manganese reduction), which we call the "methylation window."

In Hodges Reservoir, we saw this methylation window at the end of the spring season of the wet and average years (2017 and 2019), especially in 2017. MeHg production and accumulation in the hypolimnion happened from May to June (Figures 8, 9). It seems that runoff during winter–spring precipitation provided more initial mass of oxygen due to a larger hypolimnion, which delayed the onset of highly reduced conditions in bottom waters. In addition, the elevated nitrate concentration from the previous high-ammonia year, and the extra nitrate input from storm runoff, likely helped to buffer redox conditions at around 200 mV early in the season (Figures 6A,B, 7; Beutel et al., 2016). These conditions favored denitrification and microbial manganese-oxides reduction during the pre-stratified season. But with the onset of stratified conditions in May, mildly reduced conditions (0–100 mV) prevailed in bottom waters that enhanced Hg methylation by promoting inorganic Hg(II) bioavailability and SRB activity in anoxic profundal sediment. We saw a peak in MeHg accumulation rate (200–300 ng/m^2·d) overlapping with elevated manganese accumulation rate (~230 mg/m^2·d), a decrease in sulfate concentration, and low sulfide buildup in the water by May (Figure 8; Table 1), conditions known to stimulate MeHg production in aquatic systems (Gilmour et al., 2018). Other studies of Hg cycling have observed this synchronicity of elevated manganese and MeHg, suggesting that in aquatic ecosystems an increase in dissolved manganese may be the effect of mildly reduced conditions that are also suitable for anaerobic microbes able to methylate inorganic Hg(II) (Balogh et al., 2004; Gill, 2008; Alpers et al., 2014; Peterson et al., 2023).

In both years, 2017 and 2019, MeHg showed a negative MeHg accumulation rate (loss from bottom waters) late in the stratified season when the hypolimnion was highly reduced and sulfidic (Figure 8). Apparently, the methylation window closed. Two mechanisms may explain this observation: low Hg(II) bioavailability for methylation (Regnell and Watras, 2019) and elevated rates of demethylation relative to methylation (Marvin-DiPasquale et al., 2000). Experimental sediment-water chamber incubations conducted with samples from Hodges Reservoirs by Beutel et al. (2020) also observed peak MeHg accumulation rates of around 100–300 ng/m^2·d under mildly reduced conditions. MeHg accumulation rates dropped dramatically under highly reduced conditions. Fuhrmann et al. (2021) showed that methanogens were potent demethylators in reduced sediment from Hodges Reservoir, suggesting this mechanism accounts for the observed loss of MeHg in the reservoir late in the stratified season.

In contrast to the wet and average years, during the dry year of 2018, the methylation window occurred during a shorter period (Figures 7–9). With no stormwater runoff, the hypolimnion was much smaller, and reduced conditions in the water column developed earlier in the season (Figures 4, 5). As a result of the mechanisms noted above, MeHg accumulation was relatively low. A similar pattern of low MeHg accumulation throughout the stratified season, due to highly reduced and sulfidic conditions in bottom waters, was observed in Twin Lakes, Washington, United States (Beutel et al., 2014). In that lake system, oxygen addition to enhancing a stocked cold-water trout fishery unexpectedly led to an increase in Hg uptake into biota. In essence, oxygen addition may have inadvertently opened the methylation window, though MeHg uptake into biota was lower in years with elevated oxygen input compared to years with lower oxygen input.

After oxygenation in 2021, DO concentration (~2 mg/L) and redox (> 300 mV) were elevated in bottom waters during the entire sampling season (Figures 4, 5) and MeHg accumulation was absent (Figures 7, 8). The highly oxidized conditions appeared to close the methylation window, likely via inhibition of SRB activity which are obligate anaerobes and key methylators (Gilmour et al., 2018). Other potential sinks for MeHg and Hg(II) in surficial sediment include sorption to iron- and manganese-oxides, which have large surface areas and high capacity to sorb and co-precipitate with Hg species (Inoue and Munemori, 1979; Ullrich et al., 2001), and loss via aerobic demethylation (Du et al., 2019; Barkay and Gu, 2022). However, because the reservoir appeared to be more mixed after HOS operations, the low and constant MeHg concentration in the water column could be the result of sediment release followed by mixing and dilution. But whole-lake MeHg mass calculations suggest this is not the case (1.18 μg/m^3 during July 2019 versus 0.22 μg/m^3 during post-oxygenation July 2021). Thus, it appears that oxygenation did indeed suppress the accumulation of MeHg into reservoir waters, which presumably could decrease bioaccumulation in aquatic biota as well.

4.4 Management considerations

Study results highlight the role that hydrology plays in mediating nutrients, metals, and Hg cycling in Hodges Reservoir. During the wet and average years (2017 and 2019, respectively), larger water volume in the reservoir resulted in relatively low hypolimnetic concentrations of nutrients and metals but opened a window for high MeHg production under mildly reduced conditions. On the contrary, the dry year (2018) favored rapid deoxygenation of bottom waters, resulting in higher hypolimnetic concentrations of nutrients and metals but a lower accumulation rate of MeHg. This hydrology effect has implications for the reservoir's productivity and MeHg accumulation in biota. After oxygenation, water quality in Hodges Reservoir showed substantial drops in water column ammonia, phosphate, manganese, and MeHg, but elevated levels of iron and nitrate. Whole-lake TP dropped by over half when comparing pre-and post-oxygenation years (July 2019 vs. July 2021). Oxygenation also appears to lower phytoplankton productivity and its potential to produce the potent taste and odor compound geosmin.

Notwithstanding, two observations post-oxygenation merit discussion: first, the apparent loss of thermal stratification in post-oxygenation years, and second, the ongoing accumulation of some reduced compounds (e.g., manganese and iron) in bottom waters despite oxygenation. Based on temperature profiles from 2020 and 2021 (Figures 4, 5), the reservoir water column appeared to be well-mixed with no thermocline formation. This was unanticipated as cone-based HOS aims to maintain thermal stratification to allow for selective withdrawal of bottom waters free of phytoplankton and their decay by-products and to support cold-water biota in the reservoir and its tailwaters (Beutel and Horne, 1999). Numerous oxygenation cones have been used to successfully oxygenate lakes and reservoirs in the USA while maintaining stratification, including Newman Lake, Washington (max depth ~ 9.0 m) (Moore et al., 2012), Camanche Reservoir, California (max depth ~ 34.6 m) (Horne et al., 2019; Horne and Beutel, 2019), and in Indian Creek, California (max depth ~ 12.8 m) and Marston Reservoir, Colorado (max depth ~ 17.1 m) (Alex Horne, personal correspondence). Three different factors likely contributed to the mixing of the water column: the relatively shallow depth of the reservoir, the turbulent energy input from a pumped storage hydropower system, and the installation of the HOS cone at an intermediate depth (~14.5 m) rather than at the deepest point in the reservoir (~19 m).

The second observation of note was that, while dramatically affecting chemical cycling in the reservoir, HOS operation did not always maintain a well-oxygenated sediment–water interface throughout the reservoir. Rather, some chemical stratification persisted. Elevated levels of manganese and iron were seen early in the season in bottom waters during 2020–2021 (Figures 6C,D, 7). As it does not readily reoxidize to a particulate oxide under aerobic conditions, manganese is an especially good tracer of the occurrence of anoxic conditions at the sediment–water interface (Beutel et al., 2020). Hence, its persistence in bottom waters indicates reduced conditions to some extent at the sediment–water interface. Hodges Reservoir has relatively high sediment oxygen demand (~2 g/m^2·d) and during sediment-water chamber experiments, "oxic" sediment chambers still at times released nutrients and metals into overlaying water (Beutel et al., 2020). Accordingly, it is not surprising to see indications of anoxia at the sediment–water interface, even when oxygen is being added. Long-term operation of HOS at other sites has shown that sediment oxygen demand tends to decrease with time as the historic accumulation of organic matter in sediment is oxidized (Gantzer et al., 2009; Horne and Beutel, 2019). The same effect can be expected at Hodges Reservoir, though because of its extremely productive character it may take a relatively long time. Coupled with this decrease in oxygen demand should be an ability for oxygen addition to suppressing metals release more readily from profundal sediment.

Data availability statement

The raw data supporting the conclusions of this article will be made available by the authors, without undue reservation.

Author contributions

NR-M: Conceptualization, Data curation, Formal analysis, Investigation, Methodology, Software, Visualization, Writing

– original draft, Validation. MB: Conceptualization, Funding acquisition, Methodology, Project administration, Resources, Supervision, Validation, Writing – original draft, Writing – review & editing, Investigation. BF: Investigation, Validation, Writing – review & editing. SD: Investigation, Writing – review & editing. AH: Conceptualization, Validation, Writing – review & editing. SB: Funding acquisition, Resources, Validation, Writing – review & editing, Supervision. JP: Funding acquisition, Resources, Validation, Writing – review & editing, Supervision. TH: Methodology, Conceptualization, Writing – review & editing.

Funding

The author(s) declare that financial support was received for the research, authorship, and/or publication of this article. This project was funded in part by the City of San Diego with support from the California Water Board and the Environmental Systems Graduate Group at UC Merced.

Acknowledgments

We would like to thank Liying Zhao at the UC Merced Environmental Analytical Laboratory. We are grateful to all our colleagues with the City of San Diego's Public Utility District, the City of San Diego Water Quality Laboratory, and UC Merced who have contributed to our field work.

Conflict of interest

BF was employed by SePRO Corporation, EutroPHIX Division.

The remaining authors declare that the research was conducted in the absence of any commercial or financial relationships that could be construed as a potential conflict of interest.

Publisher's note

Author disclaimer

The views expressed herein are solely those of the authors and do not represent the official policies or positions of any supporting entity.

References

Alpers, C. N., Fleck, J. A., Marvin-DiPasquale, M., Stricker, C. A., Stephenson, M., and Taylor, H. E. (2014). Mercury cycling in agricultural and managed wetlands, yolo bypass, California: spatial and seasonal variations in water quality. *Sci. Total Environ.* 484, 276–287. doi: 10.1016/j.scitotenv.2013.10.096

APHA. (2023). *Standard methods for the examination of water and wastewater. 24th Edn.* Washington, DC: American Public Health Association.

Austin, D., Scharf, R., Chen, C. F., and Bode, J. (2019). Hypolimnetic oxygenation and aeration in two Midwestern USA reservoirs. *Lake Reservoir Manage.* 35, 266–276. doi: 10.1080/10402381.2019.1599087

Balistrieri, L. S., Murray, J. W., and Paul, B. (1992). The cycling of iron and manganese in the water column of Lake Sammamish, Washington. *Limnol. Oceanogr.* 37, 510–528. doi: 10.4319/lo.1992.37.3.0510

Balogh, S. J., Nollet, Y. H., and Swain, E. B. (2004). Redox chemistry in Minnesota streams during episodes of increased methylmercury discharge. *Environ. Sci. Technol.* 38, 4921–4927. doi: 10.1021/es049696c

Barkay, T., and Gu, B. (2022). Demethylation – the other side of the mercury methylation coin: a critical review. *ACS Environ. Au* 2, 77–97. doi: 10.1021/acsenvironau.1c00022

Benoit, J. M., Gilmour, C. C., Mason, R. P., and Heyes, A. (1999). Sulfide controls on mercury speciation and bioavailability to Methylating Bacteria in sediment pore waters. *Environ. Sci. Technol.* 33, 951–957. doi: 10.1021/es9808200

Beutel, M. W. (2000). *Dynamic and control of nutrient, metal and oxygen fluxes at the profundal sediment-water interface of lakes and reservoirs.* [Dissertation/Ph.D thesis] [California, CA]: University of California Berkeley.

Beutel, M. W. (2006). Inhibition of ammonia release from anoxic profundal sediments in lakes using hypolimnetic oxygenation. *Ecol. Eng.* 28, 271–279. doi: 10.1016/j.ecoleng.2006.05.009

Beutel, M. W. (2015). *Lake Hodges Reservoir Oxygen Demand Study*. Report to Brown and Caldwell and City of San Diego, June 11, 2015.

Beutel, M. W., Dent, S. R., Reed, B., Marshall, P., Gebremariam, S., Moore, B. C., et al. (2014). Effects of hypolimnetic oxygen addition on mercury bioaccumulation in Twin Lakes, Washington, USA. *Sci. Total Environ.* 496, 688–700. doi: 10.1016/j.scitotenv.2014.06.117

Beutel, M. W., Duvil, R., Cubas, F. J., Matthews, D. A., Wilhelm, F. M., Grizzard, T. J., et al. (2016). A review of managed nitrate addition to enhance surface water quality. *Crit. Rev. Environ. Sci. Technol.* 46, 1–28. doi: 10.1080/10643389.2016.1151243

Beutel, M. W., Fuhrmann, B., Herbon, G., Chow, A., Brower, S., and Pasek, J. (2020). Cycling of methylmercury and other redox-sensitive compounds in the profundal zone of a hypereutrophic water supply reservoir. *Hydrobiologia* 847, 4425–4446. doi: 10.1007/s10750-020-04192-3

Beutel, M. W., and Horne, A. J. (1999). A review of the effects of Hypolimnetic oxygenation on Lake and reservoir water quality. *Lake Reservoir Manage.* 15, 285–297. doi: 10.1080/07438149909354124

Bierlein, K. A., Rezvani, M., Socolofsky, S. A., Bryant, L. D., Wüest, A., and Little, J. C. (2017). Increased sediment oxygen flux in lakes and reservoirs: the impact of hypolimnetic oxygenation. *Water Resour. Res.* 53, 4876–4890. doi: 10.1002/2016WR019850

Bigham, G. N., Murray, K. J., Masue-Slowey, Y., and Henry, E. A. (2017). Biogeochemical controls on methylmercury in soils and sediments: implications for site management: geochemical controls on mercury methylation. *Integr. Environ. Assess. Manag.* 13, 249–263. doi: 10.1002/ieam.1822

Böttcher, M. E., and Thamdrup, B. (2001). Anaerobic sulfide oxidation and stable isotope fractionation associated with bacterial sulfur disproportionation in the presence of MnO_2. *Geochim. Cosmochim. Acta* 65, 1573–1581. doi: 10.1016/S0016-7037(00)00622-0

Chadwick, S. P., Babiarz, C. L., Hurley, J. P., and Armstrong, D. E. (2006). Influences of iron, manganese, and dissolved organic carbon on the hypolimnetic cycling of amended mercury. *Sci. Total Environ.* 368, 177–188. doi: 10.1016/j.scitotenv.2005.09.039

Chapra, S. C. (1997). *Surface water-quality modeling*. New York: WCB/McGraw-Hill, pp. 580–585.

Chen, K. Y., and Morris, J. C. (1972). Kinetics of oxidation of aqueous sulfide by oxygen. *Environ. Sci. Technol.* 6, 529–537. doi: 10.1021/es60065a008

Chikanda, F., Otake, T., Koide, A., Ito, A., and Sato, T. (2021). The formation of Fe colloids and layered double hydroxides as sequestration agents in the natural remediation of mine drainage. *Sci. Total Environ.* 774:145183. doi: 10.1016/j.scitotenv.2021.145183

City of San Diego. (2023). *Watershed Sanitary Survey*. Available at: https://www.sandiego.gov/public-utilities/water-quality/watersheds/sanitary-survey.

Cooke, G. D., Welch, E. B., and Peterson, S. A. (2013). *Lake and reservoir restoration*. Amsterdam, Netherlands: Elsevier, p. 400.

Davison, W. (1993). Iron and manganese in lakes. *Earth Sci. Rev.* 34, 119–163. doi: 10.1016/0012-8252(93)90029-7

Delfino, J. J., and Lee, G. F. (1968). Chemistry of manganese in Lake Mendota, Wisconsin. *Environ. Sci. Technol.* 2, 1094–1100. doi: 10.1021/es60023a004

Du, H., Ma, M., Igarashi, Y., and Wang, D. (2019). Biotic and abiotic degradation of methylmercury in aquatic ecosystems: a review. *Bull. Environ. Contam. Toxicol.* 102, 605–611. doi: 10.1007/s00128-018-2530-2

Eckley, C. S., Gilmour, C. C., Janssen, S., Luxton, T. P., Randall, P. M., Whalin, L., et al. (2020). The assessment and remediation of mercury contaminated sites: a review of current approaches. *Sci. Total Environ.* 707:136031. doi: 10.1016/j.scitotenv.2019.136031

Forsberg, C. (1989). Importance of sediments in understanding nutrient cyclings in lakes. *Hydrobiologia* 176–177, 263–277. doi: 10.1007/BF00026561

Fuhrmann, B., Beutel, M., Ganguli, P., Zhao, L., Brower, S., Funk, A., et al. (2021). Seasonal patterns of methylmercury production, release, and degradation in profundal sediment of a hypereutrophic reservoir. *Lake Reserv Manage.* 37, 360–377. doi: 10.1080/10402381.2021.1940397

Gantzer, P. A., Bryant, L. D., and Little, J. C. (2009). Effect of hypolimnetic oxygenation on oxygen depletion rates in two water-supply reservoirs. *Water Res.* 43, 1700–1710. doi: 10.1016/j.watres.2008.12.053

Gill, G. (2008). *Monomethylmercury photo-degradation studies. Transport, cycling, and fate of mercury and monomethylmercury in the San Francisco Delta and tributaries: an integrated mass balance assessment approach: final report to the California Department of Fish and Game and the California Bay Delta Authority, Task 5.1.* p. 21. Available at: http://mercury.mlml.calstate.edu/wp-content/uploads/2008/10/09_task5_1_final.pdf (Accessed Nov 09, 2023).

Gilmour, C. C., Bullock, A. L., McBurney, A., Podar, M., and Elias, D. A. (2018). Robust mercury methylation across diverse methanogenic Archaea. *MBio* 9, e02403–e02417. doi: 10.1128/mBio.02403-17

Gilmour, C. C., Podar, M., Bullock, A. L., Graham, A. M., Brown, S. D., Somenahally, A. C., et al. (2013). Mercury methylation by novel microorganisms from new environments. *Environ. Sci. Technol.* 47, 11810–11820. doi: 10.1021/es403075t

Golterman, H. L. (2001). Phosphate release from anoxic sediments or `what did Mortimer really write? *Hydrobiol. Sediment* 11, 99–106. doi: 10.1023/A:1017559903404

Goss, M., Swain, D. L., Abatzoglou, J. T., Sarhadi, A., Kolden, C. A., Williams, A. P., et al. (2020). Climate change is increasing the likelihood of extreme autumn wildfire conditions across California. *Environ. Res. Lett.* 15:094016. doi: 10.1088/1748-9326/ab83a7

Harris, T., Smith, V., Graham, J., Van De Waal, D., Tedesco, L., and Clercin, N. (2016). Combined effects of nitrogen to phosphorus and nitrate to ammonia ratios on cyanobacterial metabolite concentrations in eutrophic Midwestern USA reservoirs. *IW* 6, 199–210. doi: 10.5268/IW-6.2.938

Havens, S. M., Hassler, C. S., North, R. L., Guildford, S. J., Silsbe, G., Wilhelm, S. W., et al. (2012). Iron plays a role in nitrate drawdown by phytoplankton in Lake Erie surface waters as observed in Lake-wide assessments. *Can. J. Fish. Aquat. Sci.* 69, 369–381. doi: 10.1139/f2011-157

Horne, A. J., and Beutel, M. W. (2019). Hypolimnetic oxygenation 3: an engineered switch from eutrophic to a meso−/oligotrophic state in a California reservoir. *Lake Reservoir Manage.* 35, 338–353. doi: 10.1080/10402381.2019.1648613

Horne, A. J., and Goldman, C. R. (1993). *Limnology. 2nd Edn.* New York: McGraw-Hill, p. 577

Horne, A. J., Jung, R., Lai, H., Faisst, B., and Beutel, M. (2019). Hypolimnetic oxygenation 2: oxygen dynamics in a large reservoir with submerged down-flow contact oxygenation (Speece cone). *Lake Reservoir Manage.* 35, 323–337. doi: 10.1080/10402381.2019.1648612

Inoue, Y., and Munemori, M. (1979). Coprecipitation of mercury(II) with iron(III) hydroxide. *Environ. Sci. Technol.* 13, 443–445. doi: 10.1021/es60152a001

Krueger, K. M., Vavrus, C. E., Lofton, M. E., McClure, R. P., Gantzer, P., Carey, C. C., et al. (2020). Iron and manganese fluxes across the sediment-water interface in a drinking water reservoir. *Water Res.* 182:116003. doi: 10.1016/j.watres.2020.116003

Lee, R. M., and Biggs, T. W. (2015). Impacts of land use, climate variability, and management on thermal structure, anoxia, and transparency in hypereutrophic urban water supply reservoirs. *Hydrobiologia* 745, 263–284. doi: 10.1007/s10750-014-2112-1

Leung, T., Wilkinson, G. M., and Swanner, E. D. (2021). Iron availability allows sustained cyanobacterial blooms: a dual-lake case study. *Inland Waters* 11, 417–429. doi: 10.1080/20442041.2021.1904762

Liao, P., Li, W., Jiang, Y., Wu, J., Yuan, S., Fortner, J. D., et al. (2017). Formation, aggregation, and deposition dynamics of NOM-Iron colloids at anoxic–Oxic interfaces. *Environ. Sci. Technol.* 51, 12235–12245. doi: 10.1021/acs.est.7b02356

Lovley, D. R., Holmes, D. E., and Nevin, K. P. (2004). Dissimilatory Fe(III) and Mn(IV) reduction. *Adv. Microb. Physiol.* 49, 219–286. doi: 10.1016/S0065-2911(04)49005-5

Luther, G. W., Glazer, B., Ma, S., Trouwborst, R., Shultz, B. R., Druschel, G., et al. (2003). Iron and sulfur chemistry in a stratified Lake: evidence for Iron-rich sulfide complexes. *Aquat. Geochem.* 9, 87–110. doi: 10.1023/B:AQUA.0000019466.62564.94

Ma, K., Yang, R., Qu, S., Zhang, Y., Liu, Y., Xie, H., et al. (2021). Evidence for coupled Iron and nitrate reduction in the surface waters of Jiaozhou Bay. *J. Environ. Sci.* 108, 70–83. doi: 10.1016/j.jes.2021.02.016

Marvin-DiPasquale, M., Agee, J., McGowan, C., Oremland, R. S., Thomas, M., Krabbenhoft, D., et al. (2000). Methyl-mercury degradation pathways: a comparison among three mercury-impacted ecosystems. *Environ. Sci. Technol.* 34, 4908–4916. doi: 10.1021/es0013125

McCord, S. A., Beutel, M. W., Dent, S. R., and Schladow, S. G. (2016). Evaluation of mercury cycling and hypolimnetic oxygenation in mercury-impacted seasonally stratified reservoirs in the Guadalupe River watershed, California. *Water Resour. Res.* 52, 7726–7743. doi: 10.1002/2016WR019061

Mergler, D., Anderson, H. A., Chan, L. H. M., Mahaffey, K. R., Murray, M., Sakamoto, M., et al. (2007). Methylmercury exposure and health effects in humans: a worldwide concern. *AMBIO J. Hum. Environ.* 36, 3–11. doi: 10.1579/0044-7447(2007)36[3:MEAHEI]2.0.CO;2

Mitchell, A., and Balwin, B. S. (1998). Effects of desiccation/oxidation on the potential for bacterially mediated P release from sediments. *Limnol. Oceanogr.* 43, 481–487. doi: 10.4319/lo.1998.43.3.0481

Molot, L. A., Schiff, S. L., Venkiteswaran, J. J., Baulch, H. M., Higgins, S. N., Zastepa, A., et al. (2021). Low sediment redox promotes cyanobacteria blooms across a trophic range: implications for management. *Lake Reservoir Manage.* 37, 120–142. doi: 10.1080/10402381.2020.1854400

Moore, B. C., Cross, B. K., Beutel, M., Dent, S., Preece, E., and Swanson, M. (2012). Newman Lake restoration: a case study part III. Hypolimnetic oxygenation. *Lake Reservoir Manage.* 28, 311–327. doi: 10.1080/07438141.2012.738463

Morse, J. W., and Luther, G. W. (1999). Chemical influences on trace metal-sulfide interactions in anoxic sediments. *Geochim. Cosmochim. Acta* 63, 3373–3378. doi: 10.1016/S0016-7037(99)00258-6

Mosley, L. M. (2015). Drought impacts on the water quality of freshwater systems; review and integration. *Earth Sci. Rev.* 140, 203–214. doi: 10.1016/j.earscirev.2014.11.010

Munger, Z. W. (2016). *The Sources and Cycles of Iron and Manganese in Surface Water Supplies*. Virginia Polytechnic Institute. [dissertation/Ph.D thesis] [Virginia, VA]: Virginia Tech.

Payne, A. E., Demory, M. E., Leung, L. R., Ramos, A. M., Shields, C. A., Rutz, J. J., et al. (2020). Responses and impacts of atmospheric rivers to climate change. *Nat. Rev. Earth Environ.* 1, 143–157. doi: 10.1038/s43017-020-0030-5

Peterson, B. D., Poulin, B. A., Krabbenhoft, D. P., Tate, M. T., Baldwin, A. K., Naymik, J., et al. (2023). Metabolically diverse microorganisms mediate methylmercury formation under nitrate-reducing conditions in a dynamic hydroelectric reservoir. *ISME J.* 17, 1705–1718. doi: 10.1038/s41396-023-01482-1

Poulin, B. A., Tate, M. T., Ogorek, J., Breitmeyer, S. E., Baldwin, A. K., Yoder, A. M., et al. (2023). Biogeochemical and hydrologic synergy control mercury fate in an arid land river-reservoir system. *Environ. Sci.: Processes Impacts* 25, 912–928. doi: 10.1039/D3EM00032J

Regnell, O., and Watras, C. J. (2019). Microbial mercury methylation in aquatic environments: a critical review of published field and laboratory studies. *Environ. Sci. Technol.* 53, 4–19. doi: 10.1021/acs.est.8b02709

Robertson, D. M., and Imberger, J. (1994). Lake number, a quantitative Indicator of mixing used to estimate changes in dissolved oxygen. *Int. Rev. Hydrobiol.* 79, 159–176. doi: 10.1002/iroh.19940790202

Robertson, E. K., Roberts, K. E., Burdorf, L. D. W., Cook, P., and Thamdrup, B. (2016). Dissimilatory nitrate reduction Regnell to ammonium coupled to Fe(II) oxidation in sediments of a periodically hypoxic estuary: DNRA coupled to Fe(II) oxidation. *Limnol. Oceanogr.* 61, 365–381. doi: 10.1002/lno.10220

Rysgaard, S., Risgaard-Petersen, N., Niels, P., Kim, J., and Lars Peter, N. (1994). Oxygen regulation of nitrification and denitrification in sediments. *Limnol. Oceanogr.* 39, 1643–1652. doi: 10.4319/lo.1994.39.7.1643

Seelos, M., Meraz, E. R., Beutel, M. W., Traina, S. J., Furhmann, B., Burmistrova, J., et al. (2021). Evaluation of manganese oxide amendments for mercury remediation in contaminated aquatic sediments. *ACS EST Eng.* 1, 1688–1697. doi: 10.1021/acsestengg.1c00267

Søndergaard, M., Jensen, J. P., and Jeppesen, E. (2003). Role of sediment and internal loading of phosphorus in shallow lakes. *Hydrobiologia* 506-509, 135–145. doi: 10.1023/B:HYDR.0000008611.12704.dd

Ullrich, S. M., Tanton, T. W., and Abdrashitova, S. A. (2001). Mercury in the aquatic environment: a review of factors affecting methylation. *Crit. Rev. Environ. Sci. Technol.* 31, 241–293. doi: 10.1080/20016491089226

USEPA. (1996). *Method 1669: Sampling Ambient Water for Trace Metals at EPA Water Quality Criteria Levels*. United States Environmental Protection Agency.

USEPA. (2001). *Method 1630: methyl mercury in water by distillation, aqueous ethylation, purge and trap, and CVAFS. EPA-821-R-01–020. Washington, DC.* United States Environmental Protection Agency.

USEPA. (2002). *Method 1631, revision E: mercury in water by oxidation, purge and trap, and cold vapor atomic fluorescence spectrometry. EPA-821-R-02–019. Washington, DC.* United States Environmental Protection Agency.

United States Environmental Protection Agency (USEPA). (2023). *Climate Impact on Water Utilities*. Available at: https://www.epa.gov/arc-x/climate-impacts-water-utilities.

Wang, T., Zhao, D., Liu, J., Zhang, T., Wang, X., Liu, T., et al. (2023). Effects of abiotic mineral transformation of FeS on the dynamic immobilization of Cr(VI) in Oxic aquatic environments. *Sci. Total Environ.* 894, 164–991. doi: 10.1016/j.scitotenv.2023.164991

Watras, C. J. (2009). "Mercury pollution in remote freshwater lakes" in *Encyclopedia of inland waters*. ed. G. Likens (New York: Elsevier), 100–109.

Western Regional Climate Center. (2023). *Hodges Dam, California, Period of Record Precipitation (1940 to 1962)*. Available at: https://wrcc.dri.edu/cgi-bin/cliMAIN.pl?ca4014.

Wolthers, M., Charlet, L., van Der Linde, P., Rickard, S., and van Der Weiden, C. H. (2005). Surface chemistry of disordered mackinawite (FeS). *Geochim. Cosmochim. Acta* 69, 3469–3481. doi: 10.1016/j.gca.2005.01.027

World Weather Online. (2023). *Lake Hodges, San Diego Annual Weather Precipitation (2010–2020)*. Available at: https://www.worldweatheronline.com/fishing/lake-hodges-san-diego-weather-averages/california/us.aspx.

Zak, D., Kleeberg, A., and Hupfer, M. (2006). Sulphate-mediated phosphorus mobilization in riverine sediments at increasing sulphate concentration, river spree, NE Germany. *Biogeochemistry* 80, 109–119. doi: 10.1007/s10533-006-0003-x